Laboratory Measurements of the Properties of Frazil Ice Particles and Flocs in Saline Water

by

Christopher Charles Schneck

A thesis submitted in partial fulfillment of the requirements for the degree of

Master of Science

in

Water Resources Engineering

Department of Civil and Environmental Engineering
University of Alberta

Abstract

Measurements of the size and shape of frazil ice particles and flocs in saline water and of frazil ice flocs in freshwater are limited. This study consisted of a series of laboratory experiments producing frazil ice at salinities of 0 ‰, 15 ‰, 25 ‰, and 35 ‰ to address this lack of data. The laboratory set-up consisted of a large tank in a cold room with bottom mounted propellers to create turbulence. A high resolution camera set-up was used to capture images of frazil ice particles and flocs passing through cross polarizing lenses. The high resolution images of the frazil ice were processed using a computer algorithm to differentiate particles from flocs and determine key properties including size, shape, and volume.

The size and volume distributions of particles and flocs at all four salinities were found to fit lognormal distributions closely. The concentration, mean size, and standard deviation of flocs and particles were assessed at different times during the supercooling process to determine how these properties evolve with time. Comparisons were made to determine the effect of salinity on the properties of frazil ice particles and flocs. The overall mean size of frazil ice particles in saline water and freshwater was found to be similar, however qualitative observations showed that frazil ice particles in saline water tend to be more irregularly shaped. The overall mean size of frazil ice flocs in freshwater was significantly larger than in saline water. This resulted in frazil ice flocs in freshwater having a tendency to rise to the surface during the experiments whereas the saline water flocs tended to

stay suspended in the flow until the end of the experiment. Estimates for the porosity of frazil ice flocs were made by equating the estimated volume of ice produced based on thermodynamic conditions to the estimated volume of ice determined from the digital images. The estimated porosities of frazil ice flocs were determined to be 0.86, 0.82, 0.80, and 0.75 for 0 ‰, 15 ‰, 25 ‰, 35 ‰ saline water, respectively.

Acknowledgements

The author would like to express his sincerest appreciation for the guidance and direction provided by his supervisor Dr. Mark Loewen. The assistance provided throughout all aspects of this research is greatly valued. Thank you to Dr. Paul Myers for being on the examining committee and Dr. Evan Davies for chairing the exam.

The author would like to thank Perry Fedun for ongoing assistance with the experimental set-up. Thank you to Dr. Nicolas Beier for facilitating access to the cold room facility. Thanks you to Vincent McFarlane and Graeme Byer for assistance with experiments and programming

This research was supported by Natural Sciences and Engineering Research Council of Canada (NSERC), and is gratefully acknowledged.

The author would also like to thank his family and friends for their love and support throughout the graduate program. Finally, thank you to all my colleagues in the water resources department.

Table of Contents

List of Tables

List of Figures

1 Introduction

In northern rivers, the adhesive properties of frazil ice can cause the blockage of trash racks on municipal and industrial water intake structures and hydroelectric generating facilities (Morse and Richard 2009). These blockages can lead to stopped or reduced operations, which can have significant economic implications. Furthermore, frazil ice can attach to bed of the river and form anchor ice which upon its release can transport sediment downstream (Kalke et al. 2017). Large accumulations of anchor ice on the bed called anchor ice dams can impact the hydraulics of the river and lead to localized flooding (Dubé et al. 2014). Flow through hydroelectric facilities, for instance, BC Hydro facilities on the Peace River, may need to be restricted during freeze-up to promote stable ice cover downstream to prevent freeze-up ice jam flooding in downstream communities (Jasek and Pryse-phillips 2015). Similar restrictions to flow through the hydroelectric facilities may be required during a dynamic break-up to prevent break-up ice jam flooding in downstream communities. The warmer water being released downstream of hydroelectric facilities can result in open water and continuous frazil production throughout the winter, causing the ice front to actively move throughout the winter season. Accurately predicting the location of the ice front using river ice models is important for hydroelectric operations.

In oceans in Polar Regions, frazil ice plays a role in both sediment transport and sediment scour. Suspended sediment and biological colonies will attach to frazil ice particles and thus be contained in the ice cover when it becomes consolidated (Martin 1981). Understanding the shape and size of frazil particles and flocs could improve modelling of frazil ice production in the ocean because the size and shape of the crystals affects their behavior with respect to buoyant and drag forces (Matsumura and Ohshima 2015). Mathematical models for the formation of the frazil ice in the ocean often assume a single crystal size for frazil ice particles (e.g.. Jenkins Galton-Fenzi et al. 2012, Matsumura and Ohshima 2015).

In saline water, very few observations of individual frazil ice particles and frazil ice flocs have been made. Several studies have investigated the size distribution of individual frazil ice particles in freshwater. For the properties of frazil ice flocs in freshwater, limited research exists. In this study laboratory measurements of frazil ice particles and flocs in water at salinities 0 ‰, 15 ‰, 25 ‰, and 35 ‰ were conducted. Measurements of the size and shape of individual frazil ice particles and frazil ice flocs in saline and freshwater can be applied to improve river ice models and sea ice formation models.

2 Background and Literature Review

Frazil ice particles are small crystals that form when water is supercooled and turbulent. Given these conditions, frazil ice production and growth is a naturally occurring process that may be observed in rivers and oceans (Martin 1981). In northern rivers, the individual frazil ice particles that form are transported by the turbulent flow and begin to collide with one another. These collisions and the adhesive properties of the ice cause them to sinter together into groups of particles known as frazil flocs in a process known as flocculation. Sintering is the process by which particle and flocs bind together and adjust their shape in order to minimize free surface energy (Hobbs 1970). Once these frazil flocs reach a mass large enough for their buoyancy to overcome the entraining turbulence of the flow, the flocs will rise to the surface of the river. At the surface, the flocs continue to combine and form slush that then freezes together due to the cold air to form frazil pans or pancake ice. The pans will move with the flow of the river and continue to collide and combine with other pans to form larger ice floes known as rafts. Once a critical concentration of the rafts and pans has been reached on the river, a congestion or arrest of incoming ice rafts and pans will occur in a process known as bridging (Beltaos 2013). Bridging often occurs where there is a flow constriction (i.e. at a bridge or island) or at a bend in the river. Incoming ice from upstream will continue

to be arrested by the bridge until a solid ice cover is formed, and the solid ice cover will propagate upstream (Beltaos 2013). Once the solid ice cover has been formed, the layer of ice provides insulation from the cold air to the water flowing beneath, thereby preventing supercooling of the water column and preventing frazil ice production for the remainder of the winter (Beltaos 2013).

In oceans, similar conditions of supercooling and turbulence are necessary for frazil ice production to begin. In polar regions, there are two common sets of conditions that produce different types of ice cover in the ocean (Weeks 2010). The first is calm winds, cold air temperatures, and little swell, and in this case, frazil ice starts to form and freeze together into a continuous skim ice on the sea surface. The second set of conditions that produce frazil ice are cold air temperatures with appreciable swell, waves, wind, and blowing snow (Weeks 2010). As ice production begins, frazil ice forms a slurry layer on the surface and as more ice is added to the layer, the viscosity of the layer continually increases. This layer of soupy, viscous ice that forms is called grease ice. Grease ice is very flexible and weak and would not hold its shape if removed from the water. Under conditions of heavy snow, a snow water mixture can form on the surface of the ocean, which is indistinguishable from grease ice. Pancake ice, similar to rivers, has also been observed in the ocean (Weeks 2010). Frazil ice particles have been observed to deposit under sea ice, grow in situ and contribute to its thickness (Langhorne et al. 2015). These crystals known as platelet ice are characterised as fragile and dendritic in shape (Weeks 2010). There are other cases where frazil ice has been observed to form in the oceans including in open water leads or polynyas and between waters of different salinities (Martin 1981). At the mouths of rivers, the salinity difference between the ocean and the river can lead to frazil ice production (Martin 1981). The temperature difference between the saline water and freshwater can lead to supercooling of the freshwater resulting in the production of frazil ice.

Open water leads and polynyas play an important role in ice production and brine production in the ocean (Weeks 2010). As frazil ice forms in a polynya, the salt is rejected by the ice resulting in higher salinity which depresses the freezing point even further and results in colder water in the vicinity of the polynya. Most commonly, polynyas form in coastal areas, so once this cold dense water forms it can exit the shelf by a variety of mechanisms. The cold, salty water produced by polynyas may be a source of Antarctic Intermediate and Bottom Water (Weeks 2010). Antarctic Intermediate Water is a cold, relatively low salinity found at intermediate depths, and Antarctic Bottom Water is the cold saline lower layer of the world ocean. Similar conditions exist in the Artic regions where Cavalieri and Martin (1994) found that the rejection of salt during frazil ice production in polynyas in the Canadian Arctic contribute to the cold salty water in the Arctic halocline. In the polynya located in the Chukchi Sea off Cape Lisburne and Point Hope, Alaska, rapid ice growth occurs and is accompanied by an ocean salt flux that produce a dense outflow on the ocean floor (Martin 1981).

Several laboratory and field studies have reported measurements on the size and shape of individual frazil ice particles in freshwater. The reported range of diameters of disc shaped particles of 23 μm to 5 mm and lognormal particle size distributions in laboratory studies (Gosink and Osterkamp 1983, Daly and Colbeck 1986, Ye et al. 2004, Clark and Doering 2006, McFarlane et al. 2015) and field studies (Gosink and Osterkamp 1983, McFarlane et al. 2017). McFarlane et al. (2015) determined in freshwater laboratory experiments that 75 % of objects were disc-shaped with the other 25 % consisting of flocs and irregular shaped particles.

Upward-looking sonars have recently been used to estimate the size of frazil ice particles in rivers. Particle diameters ranging between 0.12 mm to 1.6 mm have been reported in these studies (Richard et al. 2011, Ghobrial et al. 2013, Marko et al. 2015). These instruments do not take direct measurements of frazil ice particles. Acoustic scattering models are used to convert acoustic signals into estimates of

the particle sizes and concentration. However, these sonar measurements have never been validated by making simultaneous independent measurements of frazil ice properties for comparison.

A limited number of measurements of the shape and size of individual frazil ice particles in saline water have been performed, but no studies have reported particle size distributions. Laboratory experiments performed by Kempema et al. (1993) reported disc diameters of 1 to 5 mm in fresh water and 1 to 3 mm in water at salinities of 29.14 ‰ and 32.00 ‰. In lab experiments with salinities between 36 ‰ and 38 ‰, Smedsrud (2001) reported an average diameter of irregular shaped frazil ice particles of 2 mm. Disc shaped particles measuring approximately 1 mm in diameter were reported in laboratory experiments at a salinity of 35.5 ‰ by Martin and Kauffman (1981). Ushio and Wakatsuchi (1993) performed laboratory experiments investigating the effect of wind conditions and salinity on the properties of frazil ice particles and found that under windy, high salinity conditions dendritic crystals having diameters of 2 to 3 mm were produced, and under calm air, lower salinity conditions disc shaped crystals with diameters of approximately 5 mm were produced. In summary, in saline water, the individual frazil ice particle sizes reported are comparable to freshwater observations, and there is a consensus that individual frazil ice particles are more irregularly shaped in saline water.

A small number of studies have been performed to investigate the process of flocculation and the properties of frazil ice flocs. Experiments suggest that frazil ice is less adhesive than freshwater frazil ice, resulting in less tendency to flocculate (Hanley and Tsang 1984, Kempema et al. 1993). Hanley and Tsang (1984) performed laboratory experiments in a tank with turbulence created by a propeller with 44 ‰ water. They observed that saline water flocs would disperse and break apart when passing near the propeller and that at the surface the frazil had no detectable resistance to force applied by a finger. This was attributed to the salt rejection that occurs when the frazil ice is formed in saline water. As the salt is

rejected by the frazil ice, it forms a thin layer of slightly higher salinity water around the frazil ice particle (Hanley and Tsang 1984). The freezing point of the saline water around the particle will then be slightly reduced and this inhibits the ability of the ice to grow and adhere to neighboring particles and flocs. Kempema et al. (1993) created flocs in a racetrack flume powered by propellers in a walk-in freezer. The study described the flocs as a group of particles aligned with their flat surfaces in contact. The flocs in saline water were also observed to be smaller on average and more dendritic in appearance when compared to freshwater flocs (Kempema et al. 1993). Flocs were observed to stay suspended in the flow and did not rise to the surface until the experiment was stopped and the turbulence subsided. In Clark and Doering's (2009) freshwater experiments in a counter rotating flume, measurements of the size of frazil ice flocs were made. In the study, a floc was defined as a group of particles that have sintered together, however, only objects with major axis of the fitted ellipse larger than 17 mm were considered flocs. They found that higher levels of turbulence intensity tended to inhibit the formation of large frazil flocs.

3 Experimental Set Up and Method

3.1 Experimental Set-Up

Experiments were performed in the frazil ice production tank in the University of Alberta's Cold Room Facility. Figure 1 provides an image of the overall set-up for the experiments. A large tank was constructed with base dimensions of 0.8 m by 1.2 m. The bottom and two sides of the tank were constructed out of stainless steel. The two additional sides were constructed out of glass, and the top of the tank is uncovered leaving the water exposed to the air. The tank was filled to a depth of 1.2 m, and four bottom-mounted propellers generated turbulence in the tank. The propellers are driven by four NEMA 34 DC variable speed electric motors (278 W, 1.514 N-m of torque, max speed of 1750 rpm). The turbulence intensity was held constant for all experiments by keeping the propeller speed constant at 325 rpm for

all experiments. In a similar series of experiments in the same tank, McFarlane et al. (2015) found that the tank-averaged turbulent kinetic energy dissipation rate was 336 cm^2/s^3 at a propeller speed of 325 rpm, and this fell within the range of dissipation rates estimated for rivers in Alberta. The speed of each motor was verified using a laser tachometer to measure the rpm.

Digital images of frazil ice were captured using a Nikon D800 with 36 megapixel resolution. The camera was equipped with as AF Micro-Nikkor 60 mm f/2.8D lens. Frazil ice particles and flocs were illuminated by a Genaray SpectroLED Essential 360 Daylight LED Light (3,200 lux at 1.0 m, 360 LED bulbs, 29.8 cm by 29.8 cm) or an Andoer FalconEyes RX-18TD 504 pcs LED Light (3660 lux at 1 m, 504 LED bulbs, 70.0 cm by 46.0 cm) that was placed on the far side of the tank. Two Cavision glass polarizers were mounted on the opposite side of the tank from the lights, on the inside of the glass (see Figure 1). Two different polarizer configurations were used for the experiments. The first configuration was two 10 by 10 cm polarizing lenses spaced 2.2 cm apart. The second configuration was two 16 by 16 cm polarizers spaced 3.5 cm apart. In both cases, the polarizers were installed at 90° to one another in order to cross polarize the light passing through. The polarizers were mounted as close as possible to the glass sidewall to prevent any distortion of the images caused by suspended frazil ice getting between the sidewall and the polarizers. A space heater was used to blow hot air against the outside of the glass sidewall to prevent frost formation.

The temperature of the water in the tank during the experiments was recorded at a rate of 0.62 Hz using a Sea-Bird SBE 39 temperature recorder (accuracy of ± 0.002°C). The temperature sensor was mounted in the tank and placed at the approximate center of the tank. Real-time water temperatures measured by the Sea-Bird were displayed on a laptop located just outside of the cold room. Spatial and temporal variations of air temperature in the cold room were measured and logged using RBR Solo Temperature Loggers (accuracy of ± 0.002°C) at a frequency of 1

Hz. Most of the heat loss was assumed to occur through the water surface so the air temperature sensors were mounted just above the water surface.

A series of experiments was performed in freshwater to determine if the water in the tank was mixed well enough that the water temperature was approximately uniform in the tank at a propeller speed of 325 rpm. Six RBR Solo temperature loggers were placed at locations throughout the tank as illustrated in Figure 2. The propellers were turned on to mix the water in the tank, and then the temperature loggers were programmed to begin sampling. The temperature in the cold room was then turned down to -10 °C and a typical supercooling event commenced. At the start of the experiment, the water temperature was approximately 1.8 °C, and the temperature was recorded for approximately 3 hours which captured the entire supercooling event. The data was sampled from the RBR Solos at a rate of 1 Hz and from the Sea-Bird at rate of 0.62 Hz. The temperature difference between each RBR Solo and the Seabird was computed at each time step throughout the experiment and these differences were then averaged over the entire event duration. The mean differences ranged from - 0.00337 °C to 0.00482 °C indicating that the temperature was approximately uniform. It is noteworthy that the average temperature difference between the Sea-Bird at the center of the tank and the RBR Solo at the location of the polarizers (75680) is 0.00067 °C, which is less than the accuracy of the RBR Solos and Sea-bird (± 0.002°C). This indicated that the temperature measurements taken at the center of the tank using the Sea-bird are reflective of the conditions at the location where the frazil ice images were taken. It is also important to note that the observed temperature differences are approximately an order of magnitude smaller than the maximum supercooling temperatures observed in this study.

Preliminary experiments were performed to determine the camera settings and location that provided the best quality images, with regards to brightness and clarity

for the three different experimental cases. The three cases were freshwater experiments using small polarizers, saline water experiments using small polarizers, and freshwater experiments using large polarizers. A summary of the camera settings and locations for the three set-ups used for each case can be found in Table 2. The distance between the camera lens and the glass sidewall of the tank was 5.7, 8.7 and 30 cm, resulting in an average pixel size of 6.4, 8.3 and 28.8 μm, respectively for the three set-ups. These pixel sizes correspond to average field of view dimensions (width by height) of 47.5 mm by 31.7 mm, 61.3 mm by 40.9 mm, and 162.9 mm by 141.3 mm, respectively for the three set-ups.

Set-up 1 was used to acquire images to estimate the properties of individual frazil ice particles in freshwater using small polarizers. However, after reviewing the captured images it was determined that the 2.2 cm spacing prevented many flocs from advecting between the polarizers or the flocs were too large for this field of view. Set-up 2 was used to capture images to measure the properties of individual frazil ice particles and flocs in saline water using large polarizers. The flocs in saline water were observed to be small enough that the 2.2 cm spacing between the polarizers did not restrict their movement and the flocs were small enough to fit in this field of view. Set-up 3 was used to capture images used to measure the properties of frazil ice flocs in freshwater using large polarizers. In this case the 3.5 cm spacing and larger field of view were sufficient to accommodate the larger freshwater flocs. The measuring volume, defined as the volume between the polarizers within the camera's field of view, for Set-up 1, 2 and 3 was 33.1, 55.1 and 805.7 cm^3, respectively.

The tank was filled with fresh, filtered tap water to a depth of 1.2 m for all experiments. The tap water was filtered using as Aqua-Pure AP110 filter with a filtration rating of 5 microns. Saline water experiments were performed at salinities of 15 ‰, 25 ‰ and 35 ‰. A salinity of 35 ‰ was chosen because it is near the upper limit of salinities found in the ocean. Intermediate salinities of 15 ‰ and

25 ‰ were chosen as they could be representative of salinities at salt-freshwater interfaces such as estuaries. Furthermore, by choosing intermediate salinities, the change in frazil ice properties as a function of salinity could be assessed. The required mass of salt was calculated and measured using a digital scale with accuracy of 0.2 g. Sifto Hy-Grade Food Grade Salt was used and is specified to be predominately sodium chloride (99.77% to 99.91% NaCl). Salinity calculations were performed based on the properties of water at 1°C, and therefore, the salt was added to the fresh, filtered water when the water temperature was approximately 1°C so that the density of water used in the calculation was consistent with the actual density of water in the tank. The propellers were then used to vigorously mix the solution until the salt was fully dissolved. Evaporation was constantly occurring in the tank so in order to ensure that the salinity remained constant during a series of experiments, the tank was periodically topped up with filtered tap water to maintain the 1.2 m depth.

It was important to hold the temperature of the air in the room approximately constant for all experiments as air temperature impacts the rate of cooling of the water. Furthermore, it was important that the air temperature stayed approximately constant during a given experiment, particularly during supercooling, to ensure a constant rate of cooling. The cold room had several limitations including regular defrost cycles causing changes in temperature of several degrees. To mitigate this issue, the time and duration of the defrost cycles were tracked and experiments were timed to avoid the defrost cycle during supercooling and ice production. Another issue was that regular maintenance activities performed by mechanical technicians were observed to impact the relationship between the programmed air temperature and observed air temperature. As a result it was observed that the programmed air temperatures did not match the actual air temperature in the cold room. Therefore, measurements of air temperature at the water surface were recorded and logged to ensure consistent air temperatures. The cold room was programmed to a temperature of -12°C during experiments taking place between January and May

2017. For the experiments occurring in September and October 2017, the room temperature was programmed at -11 °C. The mean air temperatures (± standard deviation) in the cold room were -7.95 ± 0.038 °C, -7.76 ± 0.44 °C, -8.35 ± 0.16 °C, -8.37 ± 0.16 °C and -7.69 ± 0.20 °C for the five series of experiments (i.e. small polarizer experiments at salinities of 0 ‰, 15 ‰, 25 ‰ and 35 ‰ and 0 ‰ the freshwater with large polarizers). The highest standard deviation for the air temperature in the cold room for a given experiment was determined to be ± 0.44 °C suggesting that the air temperature in the room was held constant throughout the duration of an individual experiment.

3.2 Experimental Methods

At the start of an experiment the propellers were turned on, the Sea-Bird was programmed and the polarizers were placed in the tank. For each experiment, a clear plastic ruler with an attached spacer was placed at the midpoint between the two polarizers. The camera was then manually focused on the markings and numbers of the ruler. In order to determine the approximate scale of the images, images of the ruler at the front, back, and midpoint between the polarizers were captured. Ten background images of the water in the tank prior to any ice formation were taken before each experiment. For the freshwater experiments with the small polarizers, the camera was programmed to capture images at a frequency of 1 Hz for 999 s. For the saline experiments and the freshwater experiments with the large polarizers, the camera was programmed to capture images at a frequency of 1 Hz for 1998 s. Next, the temperature in the cold room was programmed as described in Sec. 3.1 and took approximately one hour for the air temperature to stabilize to a constant temperature. Image capture started at approximately the time when the water cooled below the freezing point. During the experiments the sidewall glass and polarizers were visually monitored to ensure that no frost built up on the glass and no ice was getting in between the polarizers and the glass sidewall. Once the programmed number of images was captured, the air temperature in the room was

returned to approximately 2 °C above the freezing point to allow the ice to melt for the next day's experiment.

Repeated runs of experiments were conducted at each salinity in order reduce the uncertainty in the final results by ensemble averaging. In some cases the data from particular runs was identified as being anomalous (i.e. an outlier) as will be discussed in detail in sec. 7. After discarding these outlier runs there were 9 to 10 repeated experiments that could be ensemble averaged for each series of experiments.

During the experiment, the currents in the tank created by the propellers were strong enough to draw smaller flocs down to the bottom of the tank where they could be broken apart, which could impact the results of the experiments. The turbulence intensity was the same for all the experiments so the comparative results would not be affected by this. Furthermore, it is possible that flocs could be broken apart by interaction with the riverbed features or large swell in the ocean, so these conditions may be reasonably similar to naturally occurring conditions.

3.3 Freezing Point Depression Experiments

Supercooling curves are defined as time series plots of temperature during the time period when the temperature drops below the freezing point. An idealized supercooling curve for freshwater with a constant heat loss is presented in the upper plot of Figure 3. Initially the temperature decreases linearly with time due to the constant rate of heat loss but the slope of the curve (i.e. the rate of temperature decrease) decreases due to the heat released when frazil ice begins to form. The latent heat of fusion and the mass of ice created per unit time determine how rapidly the slope of the curve decreases, and at some point the temperature reaches its minimum value (i.e. zero slope) defined as the maximum supercooling temperature. After this point in time, the temperature continues to increases as more frazil ice is formed, and the curve eventually reaches a constant residual temperature which is

typically slightly below the freezing temperature if frazil ice production continues to occur (Hanley and Tsang 1984).

Due to the rejection of salt from the ice as the ice forms in saline water, the supercooling curves following slightly different typical patterns when comparing fresh and saline water as is illustrated in the lower plot in Figure 3. The difference is observed during the residual phase of the supercooling curve. For saline water, as ice continues to form during the residual phase the salinity of the water will continue to increase slightly, so the residual temperature of the supercooling curve will not remain constant and slightly decrease as can be seen in Figure 3 (Brescia et al. 1975). Note that the negative slope of the curve during the residual phase is exaggerated in Figure 3.

The freezing point in freshwater was assumed to be 0°C. Experiments were conducted to measure the freezing points in the saline water experiments. The experiment consisted of sampling approximately 1000 mL of water from the tank at a given salinity. This water sample was then placed in the cold room during a regular experimental run and mixed using a magnetic mixer as can be seen in Figure *4*. The water temperature in the stirred beaker was measured and logged using an RBR Solo. Supercooling curves for each of the freezing point depression experiments were plotted and the linearly sloping portion of the residual was extrapolated back to where it intersects the curve as illustrated in Figure 3. Mair et al. (1941) developed this method and though it does not provide the exact freezing point, it has been shown to produce a value accurate to within a few percent. The average of the freezing point for the experiments was taken as the freezing point for a set of experiments at a given salinity. The mean freezing point (± standard deviation) for the 15 ‰, 25 ‰, and 35 ‰ experiments were determined to be -0.89 ± 0.020 °C, -1.48 ± 0.019 °C and - 2.09 ± 0.023 °C respectively. A more complete description of these types of experiments can be found in She et al. (2016)

4 Supercooling Curves

In Figure 5 to Figure 9, the supercooling curves for all salinities and experiments are shown plotted. For a given set of experiments, the supercooling curves aligned quite well as seen in Figure 5 through Figure 9, indicating that the experimental conditions were sufficiently controlled and the results were repeatable. The negative slope that was observed during the residual of the freezing point depression experiments in saline water is not observed in the tank experiments. The quantity of ice produced in the tank relative to the overall volume of tank was not significant enough at the time the experiments were complete to reduce the freezing point enough to observe this trend.

The average maximum supercooling temperatures for the freshwater experiments using the small and large polarizers was -0.0851 °C and -0.0752 °C, respectively. The average maximum supercooling temperatures for the 15 ‰, 25 ‰ and 35 ‰ saline experiments were -0.9673 °C, -1.5652 °C and -2.1824 °C, corresponding to average supercooling values of 0.0773 °C, 0.0852 °C and 0.0924 °C, respectively.

5 Raw Frazil Ice Images

The raw images of the frazil ice particles and flocs from each experiment were visually examined to assess the qualitative differences between the saline water frazil ice and freshwater frazil ice. This analysis helped guide the development of the image processing algorithm used to compute the properties of frazil ice particles and flocs.

In freshwater experiments, the typical shape of the particles was very consistent with previously reported studies in that the individual frazil ice particles were predominantly disc-shaped. In freshwater experiments, the average size of flocs

was observed to be larger than in saline water experiments and in particular the largest freshwater flocs were significantly larger than those in saline water. Also, larger flocs in the freshwater experiments tended to rise to the surface, when the turbulence created from the propellers was still present while in saline water flocs remained in suspension until the propellers were turned off. In Figure 10, images of the different frazil ice particle shapes that were observed in the saline water experiments are presented. In saline water experiments, the shapes of individual frazil ice particles were a combination of disc, dendritic, and hexagonal shaped particles. In saline water, the largest of the frazil ice flocs were smaller than those in the freshwater, however significant difference was not observable when comparing the different saline experiments.

In Figure 11 to Figure 13, pairs of representative images taken at approximately the same time are shown to illustrate the qualitative differences between frazil ice particles and flocs in saline and freshwater at different times during a supercooling event. Images at a salinity of 35 ‰ are presented but the qualitative characteristics of the particles and flocs at this salinity are similar to those observed at the two lower salinities. The pair of images in Figure 11 illustrate the differences between frazil ice particles in saline and freshwater prior to flocculation. It is clear that in freshwater, the particles are predominately disc shaped and that in the saline water there is a wide variety of particle shapes including disc, hexagonal, dendritic and other irregular shapes. The number of particles in both images is quite sparse as ice production has just commenced at the time these images were captured.

In Figure 12, the pair of images illustrate the differences between saline and freshwater once flocculation had commenced which is shortly after the time when the minimum temperature (i.e. maximum supercooling) occurred. Similar to what was observed in Figure 11 most of the particles in freshwater are disc shaped with only a few particles in the image having irregular shapes. In saline water, a combination of disc, hexagonal and dendritic shaped particles can be observed in

the image. In both images some flocculation has commenced, and some small flocs comprised of a few particles are visible. There are many more particles and flocs visible in the images shown in Figure 12 compared to those in Figure 11.

The pair of images in Figure 13 illustrate the differences between saline water and freshwater later in the process when the heat of fusion is causing the temperature to increase and flocculation is proceeding rapidly. At this point in the process, both the saline water and freshwater images have a combination of flocs and particles. Similar to Figure 11 and Figure 12, the particles in the freshwater are predominantly disc shaped and in the saline water the particles are a combination of irregular shapes. In the saline water, there are many smaller flocs comprised largely of irregularly shaped particles that can be observed. In stark contrast, in the freshwater image, there are fewer flocs present; several smaller flocs and one very large floc that dominates the image. The very large freshwater floc is an order of magnitude larger than the largest floc visible in saline water image, and it is evident that freshwater flocs are comprised largely of disc shaped particles.

6 Image Processing

Images from each experiment were analyzed to compute the properties of individual frazil ice particles and frazil ice flocs by modifying an image processing algorithm developed by McFarlane et al. (2015). Modifications to the algorithm were made to more accurately determine particle properties for the conditions of the current set of experiments. The algorithm was also modified to distinguish between individual frazil ice particles and frazil ice flocs. Image series for each experiment were loaded into MATLAB, and the average of the ten background images were subtracted from each image in the series. The raw images from the series were then converted to grayscale using a built in MATLAB function (*rbg2gray*). This function converts the raw images to grayscale by eliminating the hue and saturation information while retaining the luminance. The grayscale

images were then converted to a binary image using a simple threshold. The threshold value is specified as a scalar luminance value between 0 and 1. As such any pixel with a scalar luminance value less than the specified threshold would be assigned a value of 0 (black) and any pixel with a scalar luminance value greater than the specified threshold would be assigned a value of 1 (white). At this point in the algorithm, the white objects correspond to frazil ice particles and flocs and the black pixels correspond to the dark ice-free background. Any objects that were touching the border of the image were eliminated from the binary image in order to prevent properties of portions of individual frazil ice particles and flocs from being computed. Finally, the white objects in the binary images were then dilated and eroded by five pixels to ensure any possible holes in the white objects had been filled in. Next, the objects that represent individual frazil ice particles or flocs were analyzed for key properties.

A MATLAB function (*regionprops*) was used to determine the area, perimeter, and centroid of each object. In addition, the major axis length, minor axis length and eccentricity of a fitted ellipse that has the same second moments as the objects were also computed. Clark and Doering (2009) assumed that the major axis length of a fitted ellipse computed in this manner was a sufficiently accurate estimate of particle and floc size in their experiments. In order to determine if this would be a valid assumption in this study, the fitted ellipses for each object in an image were plotted onto the corresponding binary image of ice particles and flocs. An example of one of these composite images is presented in Figure 14, and it is evident from this figure that the major axes of the ellipses do provide an accurate estimate of ice particle and floc sizes. The major axis length of the fitted ellipse is reported as the size of the frazil ice particles and flocs throughout this thesis. The benefit of using the properties of a fitted ellipse is that it provides an estimate of the size of the frazil ice flocs, but also information about the shape from the aspect ratio (i.e. more elongated or more circular) and orientation in space (i.e. angle of major axis relative to horizontal) of the frazil ice flocs.

One of the objectives of the image processing algorithm is to determine whether an object is a frazil ice particle or a floc. A disc shaped object will appear in an image as a circle, ellipse, or line depending on its orientation. As discussed in Sec. 5, in freshwater, frazil ice particles are almost always disc shaped and typically appear as ellipses in the raw images. As a result of this, the image processing method developed by McFarlane et al. (2015) to process images of freshwater frazil ice particles and flocs was based on the properties of the fitted ellipses. In this study, the objective of the algorithm was to determine whether an object was an individual particle, which includes both disc shaped particles and irregular shaped particles, or a floc. In general, irregular shaped particles are more elliptical in shape than frazil ice flocs so the logic behind this algorithm can be applied to this study. McFarlane et al.'s (2015) algorithm compares the perimeter and area of an object to the perimeter and area of the corresponding fitted ellipse. If the area of the object was greater than 90 % of the ellipse area, or the difference between the object perimeter and the ellipse perimeter was less than 15% the object was identified as an individual particle. The thresholds for perimeter and area were optimized by varying them to determine the values that correctly identified the highest percentage of particles and flocs. By manually checking approximately 500 individual frazil ice particles and frazil ice flocs, this method was found to correctly identify objects 94 % of the time in images taken in freshwater using area and perimeter thresholds of 90 % and 15 %, respectively. For the freshwater experiments with the small polarizers, only the properties of the individual particles were used for further analysis in this study because of reasons mentioned in Sec. 3.1. The same area and perimeter thresholds of 90 % and 15 %, respectively, were found to provide the most accurate results in the saline water. By manually checking approximately 900 individual frazil ice particles and frazil ice flocs, this method was found to correctly identify objects 90 % of the time in images taken in saline water. For the saline water experiments, the properties of the individual particles and flocs were used for further analysis in this study.

However, when this algorithm was applied to images of freshwater frazil ice captured using the large polarizer set-up it was found to have an accuracy of only 86 %. This is likely due to the fact that the pixel resolution was only 28.8 μm using the larger field of view resulting in small particles looking more irregular in shape (i.e. pixelated). As a result an additional criterion was developed to improve the accuracy of the algorithm. This criterion utilizes the ratio of the area and the perimeter of the objects (flocs or particles) and compares it to the ratio of the area and the perimeter of the corresponding fitted ellipses. The ratio of the object area to its perimeter is defined as the object area-perimeter ratio. The area A and perimeter P of the fitted ellipse were calculated using:

$$A = \pi ab \tag{1}$$

$$P \approx \pi(a+b)[1 + 3h/(10 + \sqrt{4 - 3h})] \tag{2}$$

where h is defined as:

$$h = (a-b)^2/(a+b)^2 \tag{3}$$

where a and b are semi-major and semi-minor axis length of the fitted ellipse, respectively. Equation 2 is an approximation for the perimeter of an ellipse derived by Ramanujan (1914). The ellipse area divided by the ellipse perimeter is defined as the ellipse area-perimeter ratio. The ellipse area-perimeter ratio divided by the object area-perimeter ratio is defined as the A-P parameter. If the object is a perfect ellipse, then the A-P parameter equals one. As the shape of an object becomes more different from its fitted ellipse (i.e. more irregular shaped) the A-P parameter becomes larger. The threshold for the A-P parameter used to distinguish between particles and flocs was determined, by examining a raw image and visually

identifying whether objects were particles or flocs. Approximately 500 frazil ice particles and flocs were visually identified, and the results of this manual assessment were then compared to the algorithm predictions at various thresholds. The algorithm was found to identify objects correctly 95 % of the time when the threshold was set to 1.1. That is, if an object's A-P parameter is greater than 1.1 then the object was identified as a frazil ice floc. For the freshwater experiments with the large polarizers, only the properties of the flocs were used for further analysis in this study because the resolution was insufficient to analyze the properties of individual particles.

7 Data Analysis

Application of the image processing algorithm to the images captured during each experiment provides the properties of each floc and particle that were detected in every image. This information was then used to assess how the properties of the flocs and particles change throughout a supercooling event. The mean particle or floc size and standard deviation as well as the particle or floc concentration were then computed for each image in the series. Following McFarlane et al. (2015), the noise in the resulting time series was reduced by smoothing using a 35 second moving average. In Figure 15 to Figure 22, these smoothed times series of floc and particle properties are plotted for each repeated experiment conducted at the four salinities. The time series were synchronized by aligning all the time series from each repeated experiment in a series at the time when the minimum temperature occurred.

The primary purpose of these plots was to assess the repeatability of the experiments and in particular to identify any experimental runs that were outliers. All of the mean size and standard deviation time series in Figure 15 to Figure 22 are still quite noisy for the first 500-750 s even after smoothing. This is because

prior to this time the number of particles or flocs in each image is very small (i.e. the sample size is small), and as a result, the sample size when computing the mean size and standard deviation is too small to get consistent results. If the time series from a given experiment diverged significantly from the others in the series of repeated experiments it was identified as an outlier. If an outlying experiment was discovered from these plots a detailed assessment of the raw images and supercooling conditions were examined to assess what the cause of the outlier was. The following three criteria were used to identify anomalous experiments:

- Inconsistent supercooling curves caused by cold room defrost cycles.
- Images out of focus.
- Frost build-up on the tank glass or ice between polarizers and tank glass.

This analysis found several anomalous experiments and these were discarded from the dataset. A total of 62 experiments were performed from January 31, 2017 to October 2, 2017. The goal was to repeat the experiment 10 times at each of the four salinities. After this process, there were 9 usable repeated experiments for 15 ‰, 25 ‰, 35 ‰ and freshwater for with the large polarizers, and there were 10 usable experiments for freshwater with the small polarizers. Table 3 summarizes the final experiments that were used in the study including data the maximum supercooling and cooling rates for each experiment. Despite best efforts to keep the cooling rate constant for each experiment, the limitations of using a cold room that is a commercial grade freezer made this objective challenging. The cooling rates for a given experiments ranged from 0.0086 to 0.0128 °C/min. The mean cooling rate rates were 0.0123, 0.0112, 0.0095, 0.0094, and 0.0092 °C/min for the freshwater experiments with the small polarizers, 15 ‰, 25 ‰, 35 ‰, and the freshwater experiments with the large polarizers, respectively. Figure 15 to Figure 22 show only the experiments that were used in the final analysis. In these figures, the time series of the mean size and standard deviation line up very well for all the experiments. There is a greater amount of variability in the time series of the particle or floc concentration suggesting that this property may be more sensitive to temperature variations in the cold room.

The ensemble average time series of the mean size, standard deviation and particle or floc concentration were calculated for each set of experiments at a given salinity. In order to compare these time series at the different salinities they were plotted as a function of a dimensionless time. The time of freezing is defined as the time when the water temperature reaches the freezing point. The dimensionless time is defined as the time divided by the time of cooling (t_c), which is the difference between the time of freezing (t_f) and the time when the minimum temperature (t_m) occurred as shown in Figure 23. The time of freezing t_f is taken as the origin (i.e. $t/t_c = 0$), and t_m corresponds to a dimensionless time $t/t_c = 1.0$.

Three time phases were defined to assist in comparing results at different time intervals during the supercooling. The three phases are illustrated in Figure 24 for flocs and Figure 25 for particles. Phase 1 is defined as the time from $t/t_c = 0$ to $t/t_c = 1.0$. Note that Phase 1 defines the same time interval for frazil ice particles and flocs. The other phases are defined relative to when the peak number of particles or flocs were observed in the ensemble-averaged time series following Clark and Doering (2006). Therefore, Phase 2 and Phase 3 will define different time intervals for frazil ice particles (Phase 2I and Phase 3I) and flocs (Phase 2F and Phase 3F). Phase 2F is defined as the time from $t/t_c = 1.0$ to the time where 90% of the peak number of flocs is reached (t_{90a}). Phase 3F is defined as the time from t_{90a} to the time where 90% of the peak number of particles is reached on the other side of the peak (t_{90b}) in the freshwater experiments. In the saline water experiments, the number of particles reaches a peak and stays at a value above 90% of the peak for the remainder of the time interval and therefore t_{90b} does not exist in these cases. In order to get a consistent comparison between the freshwater and saline experiment time intervals, the Phase 3F dimensionless time interval from the freshwater experiments is applied to the saline water experiments. Similarly for frazil ice particles, Phase 2I is defined as the time from $t/t_c = 1$ to the time where 90 % of the peak number of particles is reached (t_{90a}). Phase 3I is defined as the

time from t_{90a} to the time where 90% of the peak number of particles is reached on the other side of the peak (t_{90b}). The time series of the number of particles per image for saline water has a peak similar to freshwater and therefore t_{90b} is defined at all salinities.

The results from the image processing algorithm allow estimates of the volume of ice in each floc to be made by first calculating the volume of an ellipsoid as shown in Figure 26. The volume of an ellipsoid V is given by:

$$V = \frac{4}{3}\pi abc \tag{4}$$

where a and b are semi-major and semi-minor axis length of the fitted ellipse of a given floc, respectively. The dimension of a floc perpendicular to the plane of the image is unknown, and therefore c was assumed to be equal to the average of a and b. This assumption is reasonable except when the computed value of c is larger than the width between the polarizers since this is physically impossible. Therefore, for saline and fresh water experiments this constraint imposes a maximum limit on c of 2.2 and 3.5 cm, respectively. The volume of the ellipsoid was then multiplied by a factor that accounts for the porosity of the ice. There are no previous accurate estimates of the porosity of frazil ice flocs, however Beltaos (2013) suggested a porosity of 0.8 may be a reasonable estimate. Therefore, the volume of ice contained in a floc was estimated by multiplying the volume of its fitted ellipsoid by 0.2. Using these assumptions, the estimated concentration of volume of ice at the end of the principal supercooling can be calculated. A set of 25 images starting at the end of the principal supercooling were analysed, to get an average of the results at this point in time. For each image in the set of 25, the volumes of all the frazil ice flocs (i.e. volume of ice and water) were computed and the summed to determine the total volume of frazil ice flocs in the image. Then the average sum of the frazil floc volumes for the 25 images was taken to determine the average volume

of ice present at this time in the process. Once this was calculated for each individual experiment, the average floc volumes for a set of experiments (i.e. for the 35 ‰ set of experiments) was taken. The porosity was applied to the total average volume of flocs to determine the volume of ice contained in the flocs. The volume of the individual frazil ice particles was computed using a similar process assuming that the individual frazil ice particles are approximately disc shaped and using an aspect ratio of 37, which was the mean aspect ratio obtained by McFarlane et al. (2014). After computing the volumes from the individual frazil ice particles, it was determined that this quantity was insignificant compared to the volume of ice contained in the frazil ice flocs. The volume of the field of view was then calculated based on the determined pixel sizes and space between the polarizers. The ratio of the volume of ice calculated to the volume of the field of view could then be calculated which is by definition the frazil ice volume concentration.

The shape of a floc can be quantified by computing the eccentricity of its fitted ellipse. Ellipses have eccentricity between zero and one, where an eccentricity of zero corresponds to a circle and an eccentricity of one corresponds to a straight line. The eccentricity e, of an ellipse is calculated using the following equation:

$$e = \sqrt{1 - \frac{b^2}{a^2}} \tag{5}$$

where a is the semi-major axis length and b is the semi-minor axis length.

Frazil ice particle size distributions and floc size and volume distributions for all salinities were computed for each of the phases as well as the overall size and volume distribution computed by combining all three phases. The particle and floc size distributions were created by taking the sizes of all the particles in the time

interval and sorting them into 100 bins between the specified ranges of the figures to produce a histogram of the particle or flocs sizes. The histograms are plotted with the vertical axis as a percentage of the total number of particles or flocs and the horizontal axis is a lognormal scale of the size or volume. On the lognormal scale the bin sizes appear to be of equal width, however the bin sizes are actually all different sizes. The MATLAB function *logspace* was used to create visually equal sized bins on a log scale. The required inputs for this function are the lower bound of the axis, the upper bound of the axis, and number of logarithmically spaced points desired. The lower bounds were 0.01 mm, 0.01 mm, and 10^{-7} mm^3 for particle sizes, floc sizes and floc volumes, respectively. The upper bounds were 10 mm, 100 mm, and 1000 mm^3 for particle sizes, floc sizes and floc volumes, respectively.

8 Results

8.1 Frazil Ice Particle Properties

The particle size distributions at all four salinities and during each of the three phases and the overall of all three phases are plotted in Figure 27 to Figure 30. All particle size distributions closely follow a lognormal distribution at all salinities. The freshwater and 15 ‰ cases diverge the most from the lognormal distribution, whereas the 25 ‰ and 35 ‰ cases fit a lognormal distribution very closely. A summary of the mean and standard deviation of particles sizes computed from these size distributions can be found in Table 4. The overall mean size of frazil ice particles (± standard deviation) was 0.52 ± 0.4, 0.46 ± 0.35, 0.48 ± 0.33 and 0.45 ± 0.31 mm at salinities of 0 ‰, 15 ‰, 25 ‰ and 35 ‰, respectively. The mean particle sizes in freshwater were slightly larger than the mean particles sizes in saline water. The overall mean particle sizes in saline water were all very similar and do not exhibit any trend with salinity. The standard deviation decreased as salinity increased in all phases and in the overall data. Also, the standard deviation

decreased with time for all salinities, with the largest decreases observed in the freshwater and the smallest decrease observed at 35 ‰. The data in Table 4 show that for the saline experiments, the maximum mean particle size occurs during Phase 1 and decreased during the latter two phases 2I and 3I. Conversely, for the freshwater experiments, the maximum mean particle size occurred during Phase 2I.

8.2 Frazil Ice Floc Properties

The floc size distributions at all four salinities and during each of the three phases and the overall of all three phases are plotted in Figure 31 to Figure 34. All floc size distributions closely followed a lognormal distribution at all salinities and during all phases. A summary of the mean floc sizes can be found in Table 5. The overall mean floc sizes (± standard deviation) were 2.57 ± 2.88, 1.64 ± 1.63, 1.61 ± 1.43, and 1.47 ± 1.28 mm for 0 ‰, 15 ‰, 25 ‰ and 35 ‰, respectively. The mean size of the freshwater flocs was significantly larger than the saline water flocs, and this is consistent with the qualitative observations that were made during the experiments and of the raw images. The mean size of saline water flocs increased slightly with salinity but the difference in size between saline flocs and freshwater flocs is much more drastic. Similar results were found in the standard deviation for floc sizes in that the difference in standard deviation between saline and freshwater was significant. The standard deviation of the size of saline water flocs, only increases slightly as salinity decreases. At all salinities, as the experiment progressed the mean size of the flocs increased and the maximum mean size occurred during Phase 3 of the experiment.

As discussed previously it was observed that there were very large flocs present in the freshwater experiments that were not observed in the saline water experiments. In order to assess this observation quantitatively, the 95th percentile, the maximum size and the mean size of flocs larger than the 95th percentile were computed and the results are listed in Table 6. The 95th percentile of floc size was 6.91 mm in

freshwater, and decreased with increasing salinity to 3.96 mm at 35 ‰. The mean size of the largest 5 % of flocs varied from 11.9 mm in freshwater and decreased with increasing salinity to 5.38 mm at 35 ‰. The maximum floc size in freshwater was 95.1 mm which was significantly larger than any of the saline water cases. The data in Table 6 clearly supports the qualitative observation that the flocs were considerably larger in freshwater and that floc size did not vary dramatically as the salinity increased from 15 ‰ to 35 ‰.

The mean eccentricity of frazil flocs were 0.84, 0.82, 0.81, and 0.81 for 0 ‰, 15 ‰, 25 ‰, and 35 ‰, respectively. This corresponds to a ratio of major to minor axis length of 1.84, 1.75, 1.71, and 1.71 in 0 ‰, 15 ‰, 25 ‰, and 35 ‰, respectively. These eccentricity values indicate that the average shape of flocs in saline water did not vary significantly and that the average shape of flocs was slightly more elongated in freshwater compared to saline water.

The distributions for the estimated volume of ice in flocs at all four salinities and during each of the three phases and the overall of all three phases are plotted in Figure *35* to Figure 38. Similar to the frazil ice floc size distributions, the overall frazil ice floc volume distributions fit a lognormal distribution closely. During each phase, the volume distributions were also lognormal. A summary of the estimated volume of ice in flocs can be found in Table 7. The mean estimated volumes of frazil ice flocs (± standard deviation) were 8.79 ± 117.98, 1.14 ± 6.68, 0.82 ± 3.78, and 0.60 ± 2.72 mm^3 for 0 ‰, 15 ‰, 25 ‰, and 35 ‰, respectively. Given that the overall mean size of flocs in freshwater is larger when compared to saline water, it would be expected that the estimated volume of flocs in freshwater would be much larger when compared to saline water.

8.3 Evolution of Frazil Ice Properties

Figure 39 presents the ensemble averaged time series of the particle concentration, the mean particle size, and the standard deviation of the particle size at all salinities. Figure 39a presents the ensemble averaged time series of the particle concentration for all salinities. Firstly, Figure 39a shows that at all four salinities, the particle concentration initially increased, reached a peak, decreased, and then asymptotically approached a constant value. In freshwater peak particle concentration was 2.1 cm^{-3} at approximately $t/t_c = 1.20$, and in saline water the peaks were 2.2, 3.2, and 3.6 cm^{-3} at approximately t/t_c = 1.28, 1.24 and 1.23 at 15 ‰, 25 ‰ and 35 ‰, respectively. The 35 ‰ curve had the highest particle concentration throughout the entire time interval, and the freshwater curves had the lowest particle concentration throughout nearly the entire time interval, except near its peak where the freshwater curve was briefly greater than the 15 ‰ curve.

Figure 39b presents the ensemble averaged time series of the mean particle size for all salinities. Figure 39b shows that the mean individual frazil ice particle size initially increased, reached a peak, decreased, and then flattened reaching an asymptotic value of approximately 0.5 mm. The maximum mean particle size for the saline experiments occurred prior to the maximum mean particle size for the freshwater experiments. The maximum mean particle size occurred at t/t_c = 0.96 0.81, 0.79, and 0.88 for 0 ‰, 15 ‰, 25 ‰, and 35 ‰, respectively. The maximum mean in freshwater was the largest at 0.68 mm, followed by 0.63, 0.57, and 0.53 mm for 15 ‰, 25 ‰ and 35 ‰, respectively.

Figure 39c presents the ensemble averaged time series of the standard deviation of particle size for all salinities. Figure 39c shows that in saline water the three time series are very similar; the standard deviation increased from approximately 0.1 mm to 0.2 mm and then decreased until it reached a constant value of approximately 0.04 mm at approximately t/t_c = 1 until the end of the plot. The

standard deviation in freshwater is initially lower and approximately constant at a value of ~0.05 mm, then at $t/t_c = 0.6$ it started to increase and reached a peak at $t/t_c = 0.87$. After that it decreased quickly to a local minimum at $t/t_c = 1.23$ and then increased slowly up until the end of the time interval.

Figure 40 presents the ensemble averaged time series of the floc concentration, the mean floc size, and the standard deviation of floc size at all salinities. Figure 40a presents the ensemble averaged time series of the floc concentration. The shape of the curves is the same at all four salinities; the number of flocs per unit volume increased from zero initially, reached a plateau, and then remained approximately constant. In freshwater the peak floc concentration is 0.25 cm^{-3} and occurs at $t/t_c = 1.27$. For the saline water curves, they reach a plateau value and then the floc concentration stays approximately constant for the remainder of the time interval. The constant portion of the floc concentration begins at $t/t_c = 1.39$ for saline water experiments. The maximum floc concentration increased with salinity and the plateau values were 1.10, 1.37, and 1.86 cm^{-3} for 15 ‰, 25 ‰, and 35 ‰, respectively.

Figure 40b presents the ensemble averaged time series of the mean floc size for all salinities. Figure 40b shows that as time progressed, the general trend for all cases is that the mean floc size continually increased with time over the time interval. Initially (i.e. $t/t_c \leq 0.8$) the time series are noisy, particularly for the freshwater case, because only a very small number of frazil ice flocs were produced during this time, so this data is likely not significant. At $t/t_c \geq 0.8$ the floc concentration has increased sufficiently that the noise disappears in all cases. For the freshwater case, the mean floc size increased from 1.70 mm at $t/t_c \sim 1$ to 2.20 mm at $t/t_c \sim 1.13$. At this point in time, there was a dramatic decrease in slope and the mean floc size increased very slowly to 2.40 mm until $t/t_c = 2$. In saline water the slope of the curves were approximately constant over the entire time interval. The mean floc size at any

given time in saline water was approximately the same since the three curves are very similar. In saline water the mean floc size increased from approximately 1.0 to 1.90 mm as t/t_c increased from 0.8 to 2.0. The average floc size at all times was always larger in freshwater than in saline water.

Figure 40c presents the ensemble averaged time series of the standard deviation of floc size for all salinities. The time series at $t/t_c \leq 1$ were quite noisy and therefore will be disregarded in this analysis. At $t/t_c = 1$ the standard deviation curves essentially flattened out in all cases (i.e. slope of the curves ~ 0) and the values remained constant until $t/t_c = 2$. The standard deviation was slightly lower than the saline water experiments from at $t/t_c \geq 1.2$ the standard deviation varied between ~0.15 mm to ~0.25 mm with the lowest value being in freshwater.

8.4 Ice Volume Concentrations

An estimate of the ice volume concentration can be calculating by considering the thermodynamic conditions of the experiment (Osterkamp 1978). Considering a tank that is fully mixed with insulated sides and bottom with the surface exposed to the air. The frazil ice tank has sides made of glass and stainless steel, so some heat will be lost there as well, however, it will be assumed that most of the heat loss occurs at the surface of the tank (Ye et al. 2004). The total heat exchanged with the surrounding environment, Q_{tw} in W/m^3 is given by:

$$Q_{tw} = \rho C_p \frac{dT}{dt} \tag{6}$$

where, ρ is the density of water in kg/m^3, C_p is the specific heat of the water in J/Kkg, and $\frac{dT}{dt}$ is the cooling rate in K/s. Density and specific heat depend on salinity and can be calculated based on the salinity of the experiment (Gill 1982). The

cooling rate can be obtained from the supercooling curve for the experiments. The cooling rate is determined by calculating the slope of the supercooling curve over an interval starting 15 minutes before it crosses the freezing point until the time it crosses the freezing point. The volume concentration of frazil ice, M_{sp} in m^3/m^3 can be calculated using:

$$M_{sp} = Q_{tw} t_{sp} / L_i \rho_i \quad (7)$$

where, t_{sp} is the time of the principal supercooling in s, L_i is the latent heat of fusion for ice in J/kg (334 J/kg), and ρ_i is the density of ice kg/m^3 (917 kg/m^3). The time of principal supercooling can be obtained from the averaged supercooling curves and its calculation is shown in Figure 41 to Figure 44. The time of principal supercooling was 896, 1064, 1297, and 1275 s for 0 ‰, 15 ‰, 25 ‰, and 35 ‰, respectively. Based on these calculations the computed volume concentration of ice formed during the principal supercooling were 0.0019, 0.0027, 0.0028, and 0.0027 m^3/m^3 for salinities of 0 ‰, 15 ‰, 25 ‰, and 35 ‰, respectively.

The images obtained can be used to estimate the volume of ice produced during the experiments at the end of the principal supercooling as described in Sec. 7. The estimated volume concentrations for salinities of 0 ‰, 15 ‰, 25 ‰, and 35 ‰ were 0.0028, 0.0031, 0.0028, and 0.0021 m^3/m^3, respectively. These values are all slightly higher than the theoretical calculations. This indicates that assuming flocs are ellipsoid may provide a reasonable estimate of the total volume contained in flocs. In the freshwater experiments, at the end of the time of principal supercooling, the number of flocs per volume has already started to decrease due to the flocs rising out of the flow as can be seen in Figure 24 so this value of volume concentration could be slightly underestimated.

This information can also be used to estimate the porosity of frazil flocs, by equating the theoretical volume concentration of ice computed using Eq. 7 to the estimated volume concentration computed from the images. This calculation gives estimated porosities for frazil ice flocs of 0.86, 0.82, 0.80, and 0.75 for 0 ‰, 15 ‰, 25 ‰, and 35 ‰, respectively.

9 Discussion

From Table 4, the overall mean size of frazil ice particles was slightly larger in freshwater than in saline water. The overall mean particle size in freshwater of 0.52 mm falls within the reported ranges of previous studies of 23 μm to 5 mm (Gosink and Osterkamp 1983, Daly and Colbeck 1986, Ye et al. 2004, Clark and Doering 2006, McFarlane et al. 2015, 2017). The overall mean particle sizes reports in saline water of 0.46, 0.48, and 0.45 mm at 15 ‰, 25 ‰, and 35 ‰, respectively, are smaller than the previous reported estimates of particle size in saline water, which are on the order of 1 to 3 mm (Martin and Kauffman 1981, Kempema et al. 1993, Ushio and Wakatsuchi 1993, Smedsrud 2001). However, these previously reported size ranges were using very small sample sizes and using less sophisticated measuring techniques including visual observations so may have influenced the results. However, the values reported in the previous studies still fall within the range of sizes observed in this study.

The overall mean size of particles in freshwater were 1.13, 1.08, and 1.15 times larger than particles in 15 ‰, 25 ‰, and 35 ‰ saline water, respectively. This suggests that the nucleation and growth of frazil ice particles are fairly similar in fresh and saline water. The particle size distributions at all salinities were lognormal, which is further evidence that the processes involved are similar. The particle size distributions in fresh water plotted in Figure 27 have a small plateau at ~2 mm indicating that the distributions are slightly bimodal with a small secondary peak. This may be because the image processing algorithm wrongly identified some

small flocs as particles. This plateau would skew the mean slightly higher, which could be responsible for the slightly higher mean in freshwater compared to saline water as this plateau is not present in the saline water particle size distributions plotted in Figure 28 to Figure 30. Qualitative results reported in this study that particles are predominantly disc shaped in freshwater are similar to results reported in McFarlane et al. (2015) and a combination of irregular shapes and disc shaped in saline water similar to results in Ushio and Wakatsuchi (1993).

The overall mean size of frazil ice flocs in freshwater was significantly larger than in saline water (see Table 5). Past studies have reported similar qualitative results that freshwater flocs are larger and more adhesive than saline water flocs (Hanley and Tsang 1984, Kempema et al. 1993). The overall mean size of flocs in freshwater was 2.57 mm, which suggests that Clark and Doering (2009) measurements of flocs larger than 17 mm is not capturing the full spectrum of the floc size distribution. Flocs in freshwater were on average 1.57, 1.60, and 1.75 times larger than in 15 ‰, 25 ‰, and 35 ‰ saline water, respectively, suggesting that the flocculation process in saline water is significantly different than in freshwater. The difference in the flocculation process can be explained by freezing point depression in saline water. As the salt is rejected by the ice, it will increase the salinity of the surrounding water and slightly reduce the freezing point. This will inhibit the process of adhering and sintering, thus resulting in the mean size of frazil flocs decreasing with salinity. From Table 6, the 95th percentile of the floc sizes and the mean of the floc sizes larger than the 95th percentile are also largest in freshwater and decrease with salinity. The maximum floc size observed in the freshwater experiments is also significantly larger than in the saline experiments.

As expected, the volume of frazil flocs magnifies this result, as the overall mean volume of flocs in freshwater was 7.71, 10.72, and 14.65 times larger than in 15 ‰, 25 ‰, and 35 ‰ saline water, respectively. It is interesting to note that there is large difference between the floc sizes when comparing freshwater to saline water, but

the variation in saline water is less significant. This is further evidence that the flocculation process is dependent on whether the process occurs in saline water or freshwater, and less dependent on exactly how saline the water is. The floc size distributions at all salinities were lognormal. For the saline water floc size distributions, there is a secondary peak that diverges from the lognormal distribution around the 0.1 mm size as observed in Figure 32 to Figure 34. This deviation is likely a result of minor issues in the image processing algorithm that could be wrongly identifying some irregularly shaped particles as flocs. This second peak is more pronounced during Phase 1 and becomes less pronounced in the later phases because there are fewer flocs present during Phase 1.

In Figure 39a, in saline water, the higher the salinity, the higher the particle concentration curves are throughout the entire time interval. As the salt is rejected by the ice, this can create a small pocket around the ice particle with a higher salinity and slightly lower freezing point, thus inhibiting the flocculation process. This would result in less particles adhering and sintering together to form flocs, leaving more particles in suspension, and producing the observed result of more particles being present at higher salinities. All of the time series of the particle concentration in Figure 39a follow a similar pattern of increasing, reaching a peak, and then decreasing with time. This pattern can be explained by considering particle production and the flocculation process. The flocculation rate, defined as the rate at which particles are sintered to other particles or flocs, is clearly a function of the particle concentration. This is because when there are more particles there is higher likelihood of particle to particle and particle to floc collisions which present opportunities for sintering. Prior to the time when the peaks occurs in the time series in Figure 39a particle production exceeds the flocculation rate but as time progresses a point is reached where particle production equals the rate of flocculation and the peak occurs at this time. This balance is reached because the flocculation rate is increasing as can be seen in Figure 40a. It is also likely that at some time point prior to the peak the particle production begins to decrease. As

time progresses the particle production reaches an asymptotic value because the water is at the residual temperature and the flocculation rate decreases until a balance is again achieved.

From Table 4 and Figure 39a it can been seen that in saline water, the mean size of particles is the largest during the Phase 1 and smallest during Phase 3I. During Phase 1, there are fewer particles present, so there is a lower probability of collision leading to flocculation during this phase and therefore, particles have more time to grow thus resulting in larger mean particle size. It would seem reasonable to expect a similar result in freshwater; however, in freshwater, the largest mean particle occurs during Phase 2I. In Figure 39a, it can be observed that the nucleation starts sooner in the saline water experiments (i.e. particles are being produced earlier than in freshwater), and particles do not start to appear until around $t/t_c = 0.8$ in freshwater compared to $t/t_c = 0.5$ in saline water. Therefore, the particles have less time to grow during Phase 1 and reach their maximum mean size later in the process during Phase 2I.

In all experiments, the mean size and mean volume of flocs increased as the experiments progressed (see Figure 40 and Table 7). As particle production continues, the probability of collisions of particles to flocs increases, resulting in an increase of the mean floc size in all cases. Later on in the process, when the particle production slows down, most of the collisions would be particle to floc resulting in the slow steady growth of flocs until the end of the time of the experiments. If this slow growth continues beyond the time of experiments, it is possible that the saline water flocs may eventually grow as large as the freshwater flocs. This would suggest that the average rate of flocculation is slower than in freshwater. In saline water, the floc concentration curves followed a similar pattern at all salinities increasing until they reach steady state condition (i.e. slope of curve is zero). Conversely, in freshwater, the floc concentration increased, reached a peak and then slowly decreased. This can be explained by the visual observation that the

flocs in freshwater tended to rise to the surface before the experiment was completed, whereas the saline water flocs tended to remain suspended until the end of the experiment. The larger mean size of the freshwater flocs increases their buoyancy, and thus increases their ability to overcome the turbulence of the flow and rise to the surface. This result is similar to observations made by Kempema et al. (1993).

In Figure 40a, the higher the salinity, the higher the floc concentration curves are throughout the entire time interval. As salinity increases, the tendency to flocculate decreases so this result may seem counterintuitive because a lower tendency to flocculate could mean less flocs. Note that a particle to particle combination increases the floc concentration, a particle to floc combination does not change the floc concentration, and a floc to floc combination decreases the floc concentration. Perhaps in more saline water, the particle to particle combination is less affected by salinity resulting in higher floc concentrations, but with smaller sizes as previously noted. Saline water inhibits the adherence and sintering of two objects and the flocs, which are on average larger than particles, would have greater drag forces on them from the turbulence, which could decrease the likelihood of adherence and sintering when two flocs collide. These two conditions could explain the result of higher floc concentrations at higher salinities. Eventually, the floc concentration curves reach a plateau which suggests that the particle to floc combination becomes the dominant process as this combination produces a net zero contribution to the floc concentration. This is logical because at this point the particle production rate has decreased, resulting in low particle concentrations which reduces the probability of two particles colliding to near zero. However, the concentration of flocs is high, making particle floc collisions much more probable.

10 Conclusions

A total of 46 laboratory experiments were performed to determine the properties of individual frazil ice particles and flocs at various salinities. Experiments at salinities of 0 ‰, 15 ‰, 25 ‰, and 35 ‰ were performed to assess how the properties of frazil ice vary with salinity. These salinities are reflective of natural bodies of water such as oceans where the upper limit of salinity of 35 ‰, in rivers where salinity is 0 ‰, and in estuaries where intermediate salinities can occur. For this study, high resolution digital images were collected of the frazil ice particles and flocs. The images were processed using MATLAB to identify particles and flocs and determine the geometric properties including their size and shape. The algorithms corrected identified the objects as flocs or particles 90 % to 95% of the time.

The mean particle sizes were determined to be 0.52, 0.46, 0.48, and 0.45 mm for salinities of 0 ‰, 15 ‰, 25 ‰, and 35 ‰, respectively. This indicates that mean particle sizes are only weakly dependent on salinity, decreasing by only 13% as the salinity increased from 0 ‰ to 35 ‰. Visual examination of the images clearly showed that there were more irregular shaped particles in saline water than in freshwater. At all four salinities, the particle concentration increased to a peak value and then decreased until the end of the experiment. This number declines because flocculation commences and particles are being combined together into flocs and thus being removed from suspension. The interaction of the particle concentration curves and floc concentration curves clearly illustrate this process. A lognormal distribution was observed to fit all the particle size distributions closely.

The mean floc sizes were determined to be 2.57, 1.64, 1.61, and 1.47 mm for 0 ‰, 15 ‰, 25 ‰, and 35 ‰, respectively. The freshwater flocs are significantly larger on average than the saline water flocs, suggesting that the presence of salt has an impact on the flocculation process. A lognormal distribution was observed to fit all the floc size and volume distributions very well. At all four salinities, the mean floc

sizes increased as time progressed and reached a maximum mean size at the end of the experiment. The freshwater flocs were observed to rise to the surface of the tank during the experiment, whereas the saline water flocs were observed to stay suspended in the flow. In the saline water experiments, the floc concentration reached a peak and then remained approximately steady throughout the remainder of the experiment, clearly indicating that saline water flocs tend to stay suspended in the flow. Conversely, in the freshwater experiments, the floc concentration increased to a peak and then slowly declined, which supports the conclusion that freshwater flocs tend to rise to the surface quite rapidly.

The volume concentration of ice in the tank was computed from the frazil ice image analysis results by assuming an ellipsoid floc shape and a porosity of 0.80. The volume concentration of ice was also calculated using a thermodynamic approach based on the properties of the supercooling curves. Estimates of the porosity of frazil ice flocs were calculated by adjusting the porosity so that the volume concentrations computed using the two methods were equal. This analysis gave porosities equal to 0.86, 0.82, 0.80, and 0.75 for 0 ‰, 15 ‰, 25 ‰, 35 ‰, respectively. These results suggest that as salinity increases porosity decreases slightly, and that Beltaos' (2013) assumption that the porosity of frazil flocs in freshwater is 0.80 was reasonable.

In summary, the data obtained about the properties of frazil ice particles and flocs in saline water can be applied to oceanic frazil ice production models. Often times these models make assumptions about the size and shape of particles, such as assuming that the properties of saline frazil ice are the same as freshwater frazil ice or that all frazil ice particles are the same size. The data from this study can be applied to improve the assumptions made about the frazil ice particles and flocs and give more accurate model predictions. Additionally, in river ice models, the process by which particles join together to create flocs can have implications for the freeze-up processes and overall development of the solid ice cover. River ice models can

use the data reported in this study to improve the assumptions made about the properties of frazil flocs and how they rise to the water surface.

10.1 Recommendations for Future Research

Developing a camera set-up that is able to capture simultaneous photos of the flocs and particles in the third dimension would assist in validating the estimates for the shape and volume of frazil flocs. Three dimensional imaging techniques should be investigated to determine if technology exists that could capture the three dimensional shape and complex features of the flocs. These images could provide insight into the flocculation process and the means by which particles adhere to one another and sinter together.

Field studies using similar techniques to this laboratory study should be undertaken to determine the properties of frazil flocs in natural streams, estuaries and oceans. A set-up similar to that used by McFarlane et al. (2017) could be modified to capture floc properties in natural streams and particle and floc properties in the ocean.

Finally, advanced image processing techniques should be investigated to improve the identification algorithm for flocs and particles. It would be of interest to quantify the number of disc shaped particles and the number of irregular shaped particles in saline water. For example, a support vector machine learning model could be trained and applied to differentiate between irregular shaped particles and disc shaped particles.

Figures

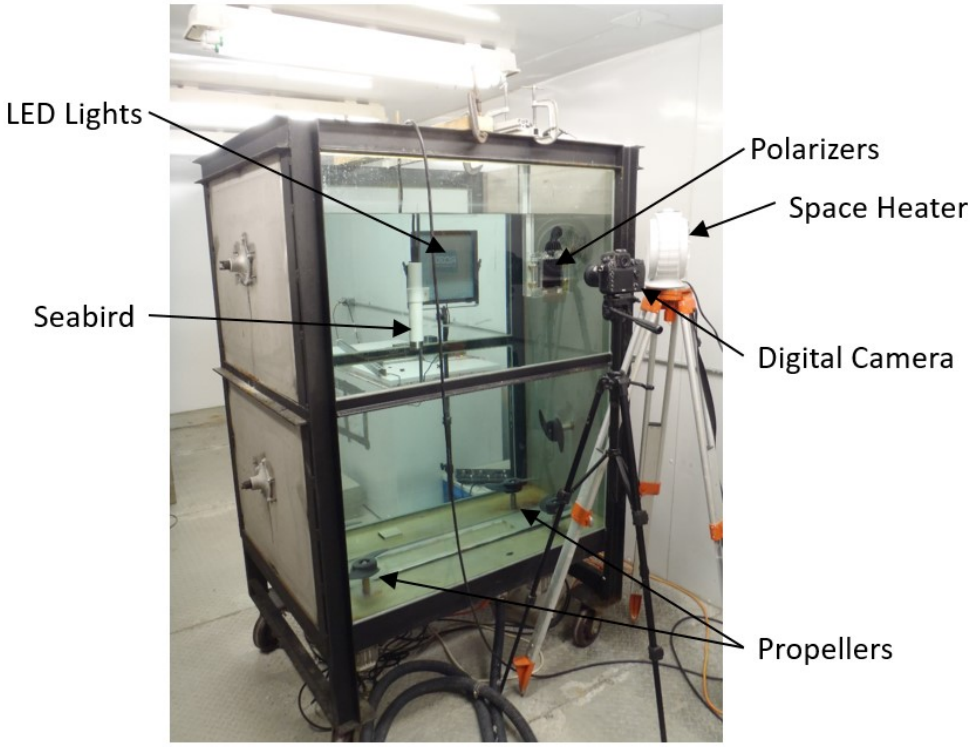

Figure 1: Image of the frazil ice tank experimental set-up.

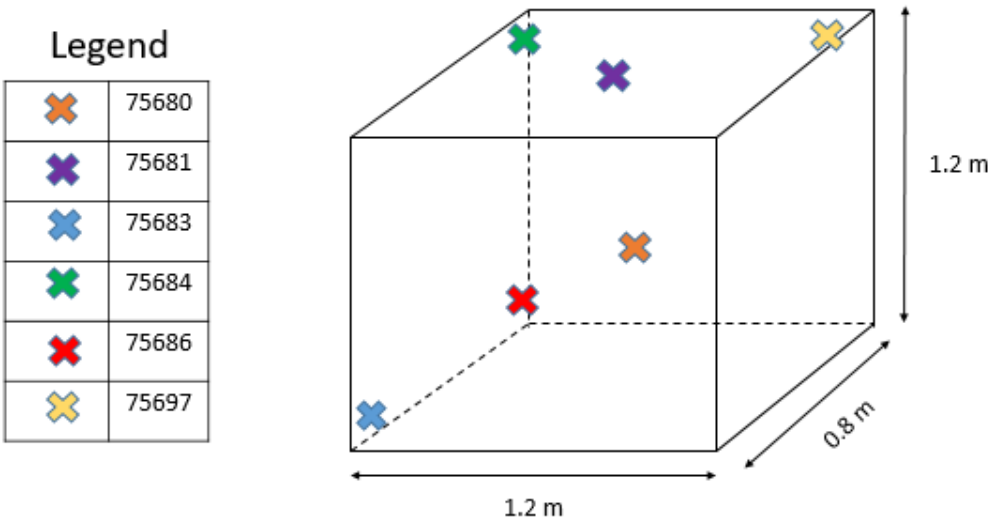

Figure 2: Location of RBR Solos for experiments measuring spatial variation in temperature in the tank. RBR Solo 75680 is located near the glass at the location where the polarizers are placed in Figure 1. RBR Solo 75681 is located near the water surface of the tank near the center. All other RBR were placed in the corners as illustrated in the figure.

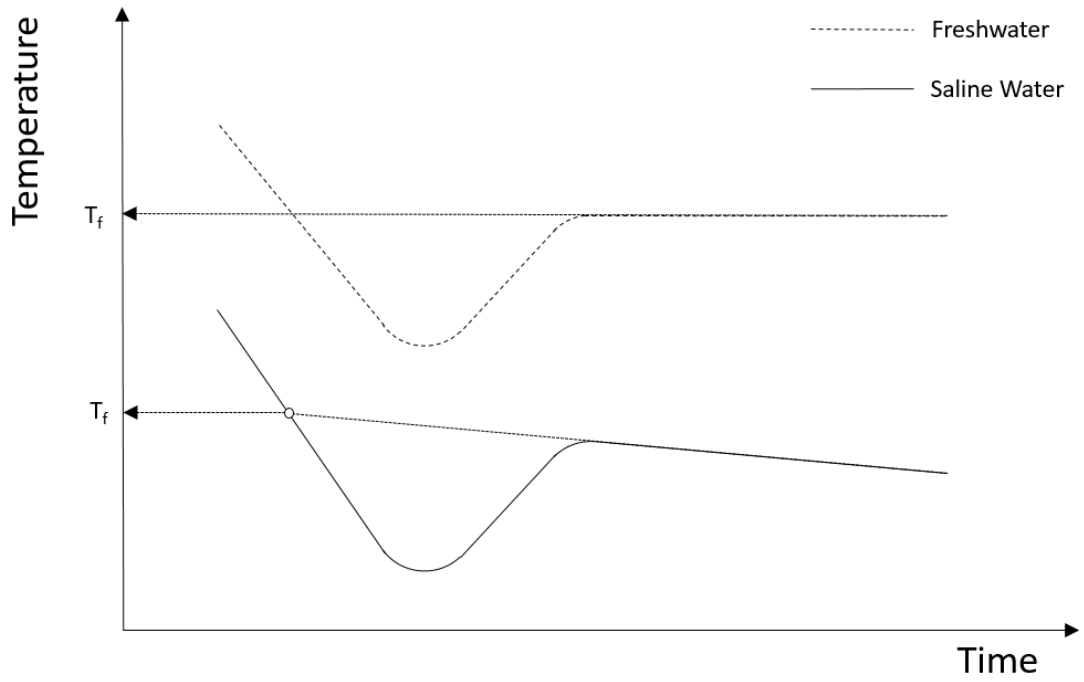

Figure 3: Typical supercooling curves in freshwater and saline water. (Adapted from She et al. (2016).)

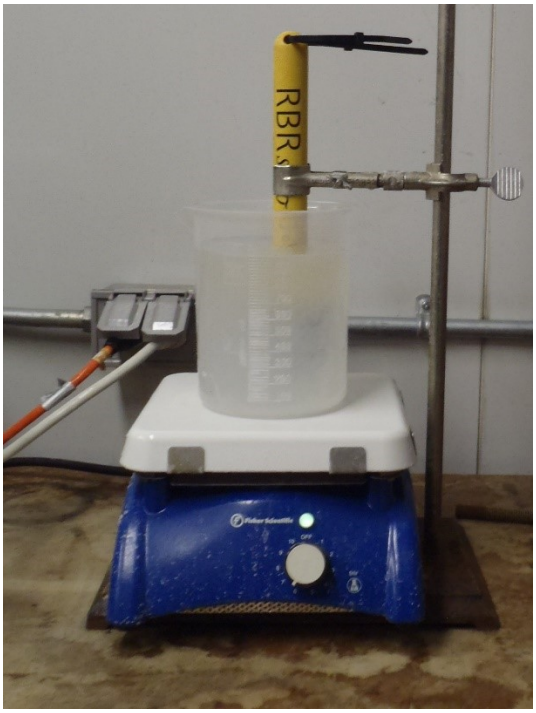

Figure 4: Image of the freezing point depression experimental set-up.

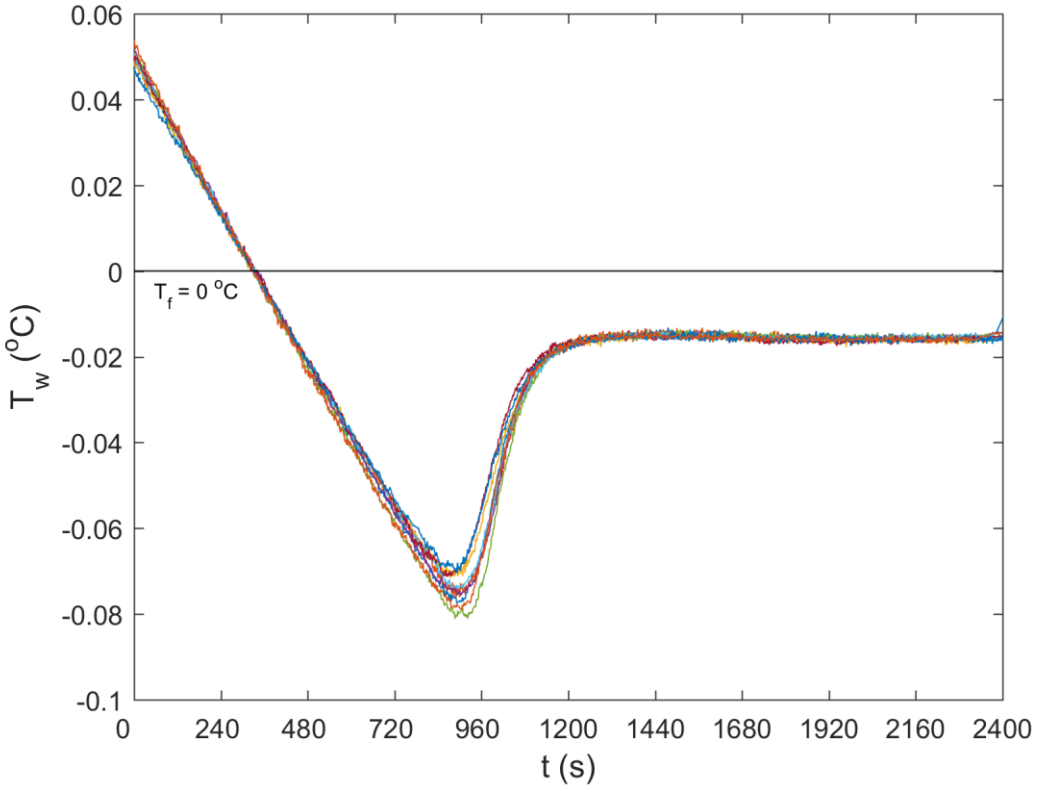

Figure 5: Superimposed supercooling curves showing water temperature, T_w, as a function of time, t, for freshwater experiments observing flocs. The freezing temperature T_f is indicated by the horizontal line.

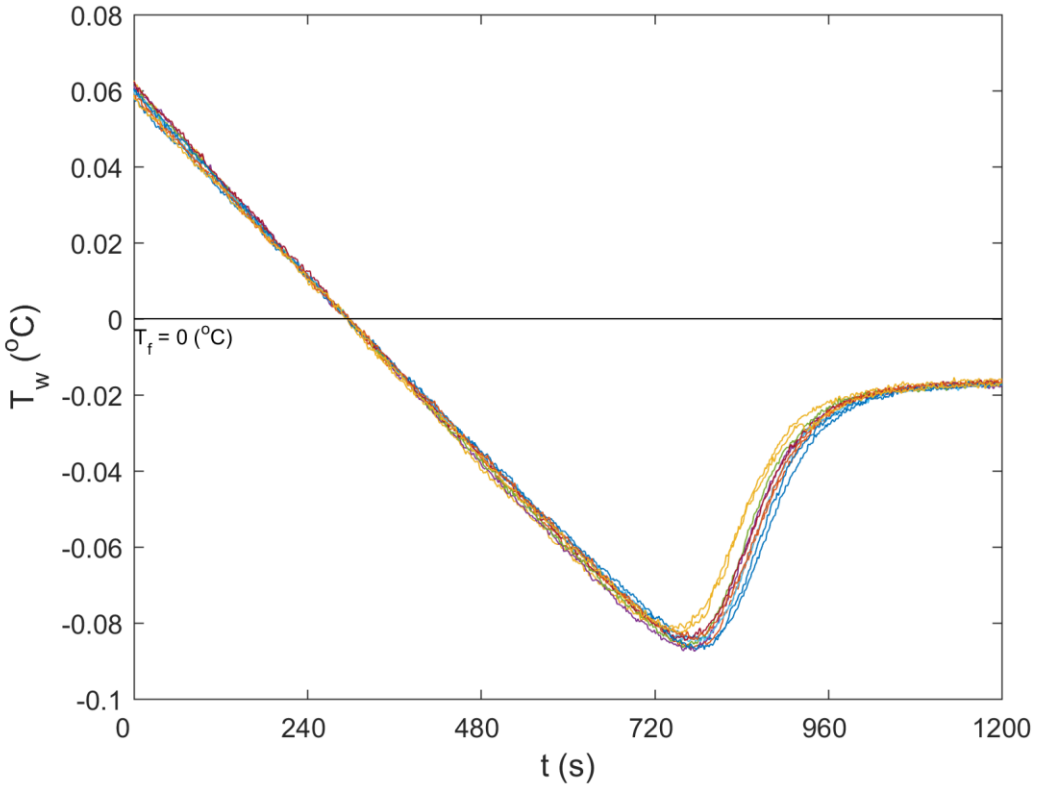

Figure 6: Superimposed supercooling curves showing water temperature, T_w, as a function of time, t, for freshwater experiments observing particles. The freezing temperature T_f is indicated by the horizontal line.

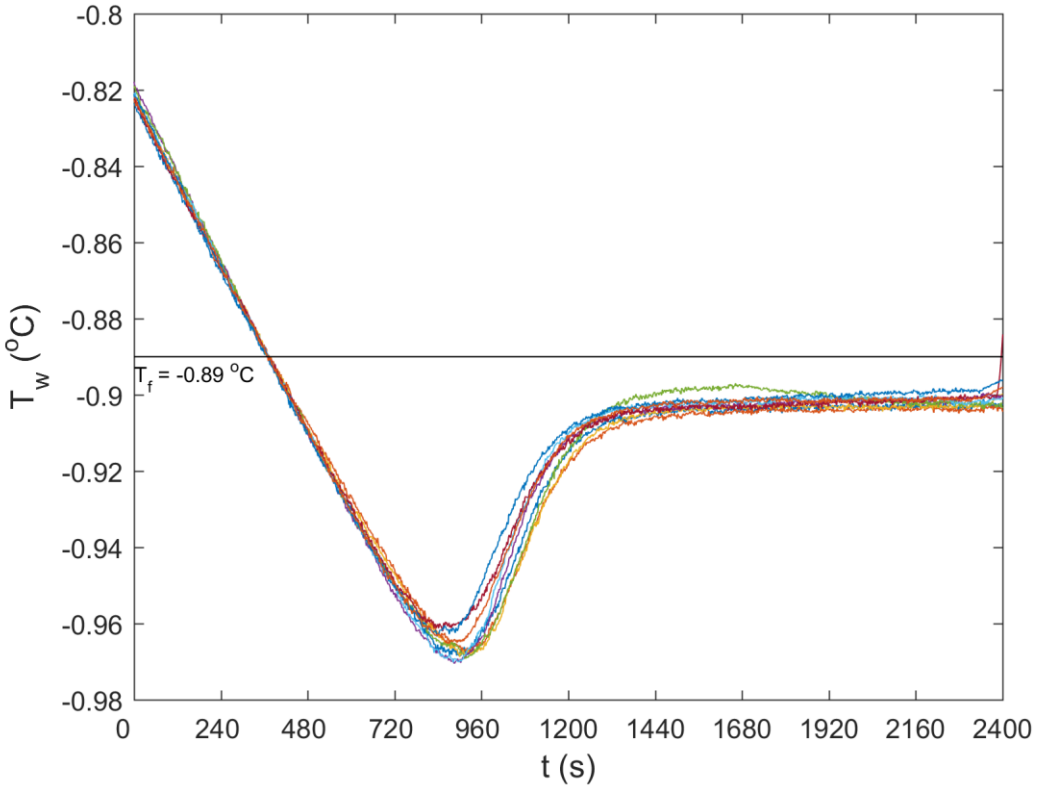

Figure 7: Superimposed supercooling curves showing water temperature, T_w, as a function of time, t, for 15 ‰ experiments. The freezing temperature T_f is indicated by the horizontal line.

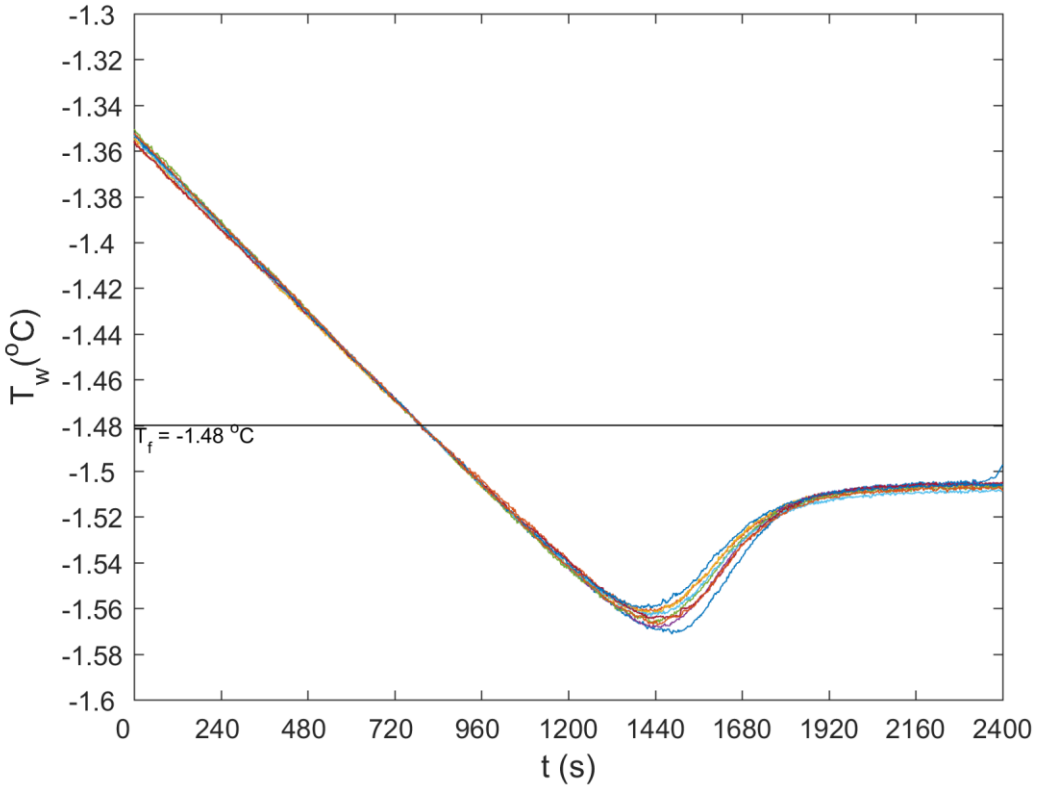

Figure 8: Superimposed supercooling curves showing water temperature, T_w, as a function of time, t, for 25 ‰ experiments. The freezing temperature T_f is indicated by the horizontal line.

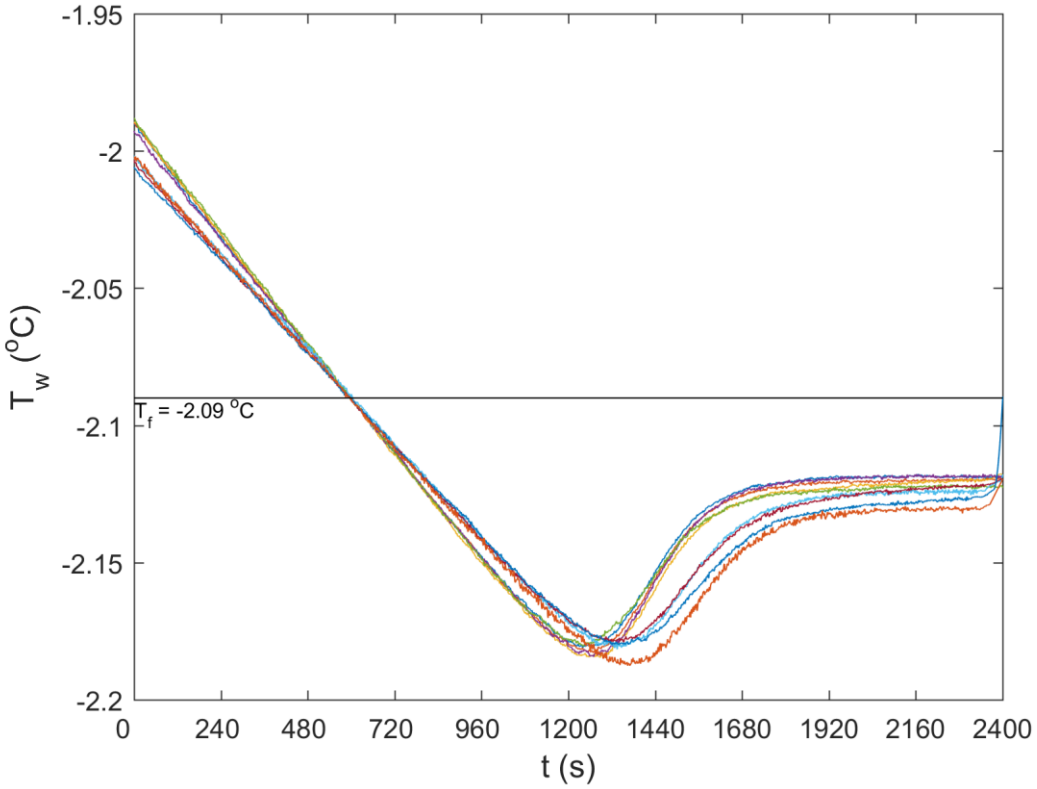

Figure 9: Superimposed supercooling curves showing water temperature, T_w, as a function of time, t, for 35 ‰ experiments. The freezing temperature T_f is indicated by the horizontal line.

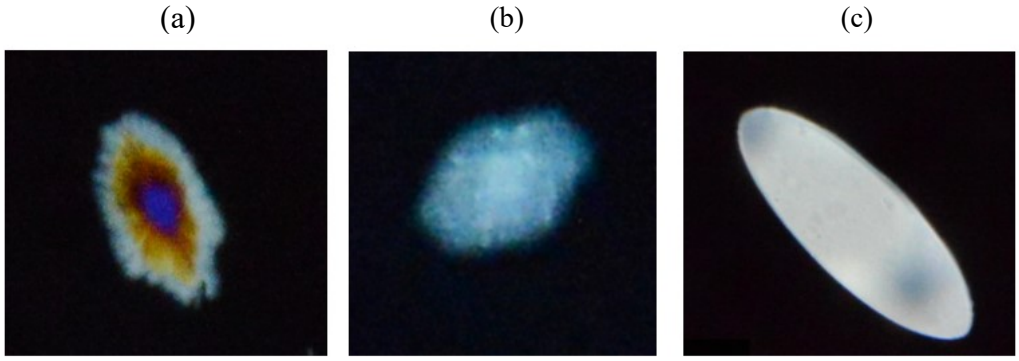

Figure 10: Zoomed in images of different shaped particles. a) dendritic, b) hexagonal, and c) disc shaped particles.

(a)

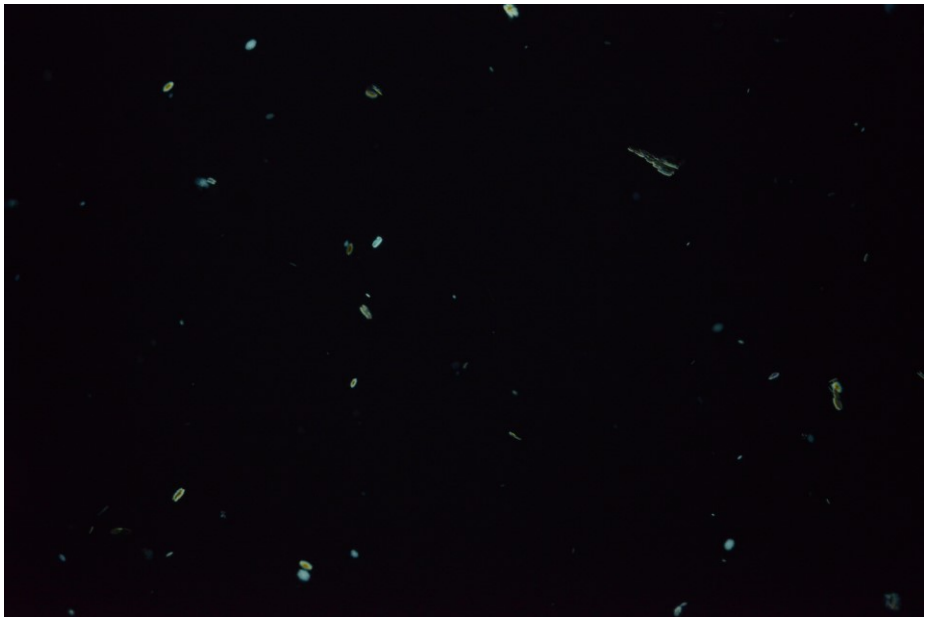

(b)

Figure 11: Raw digital images taken prior to flocculation (a) 35 ‰ and (b) freshwater. Image dimensions are 3.07 cm by 4.61 cm.

(a)

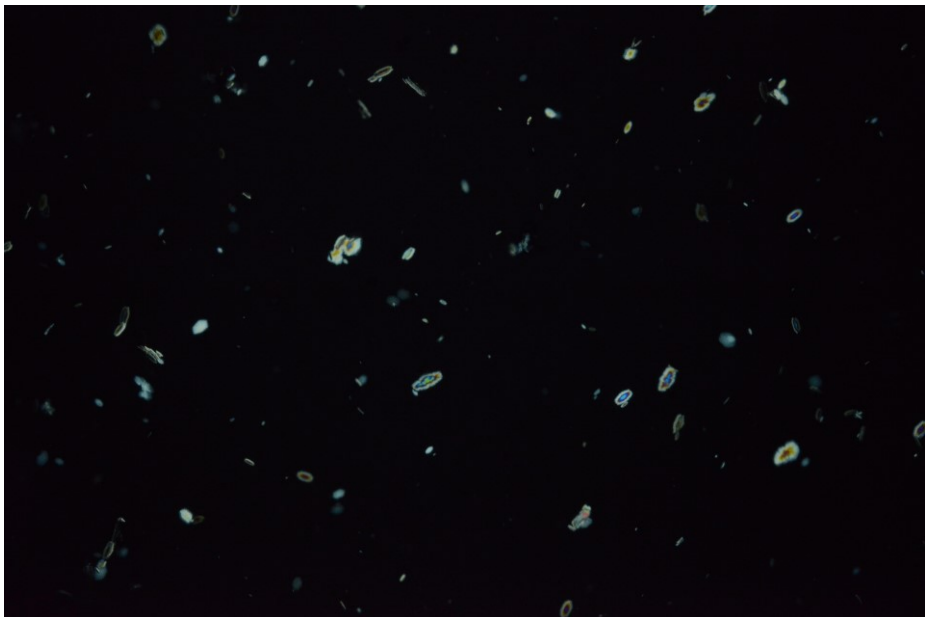

(b)

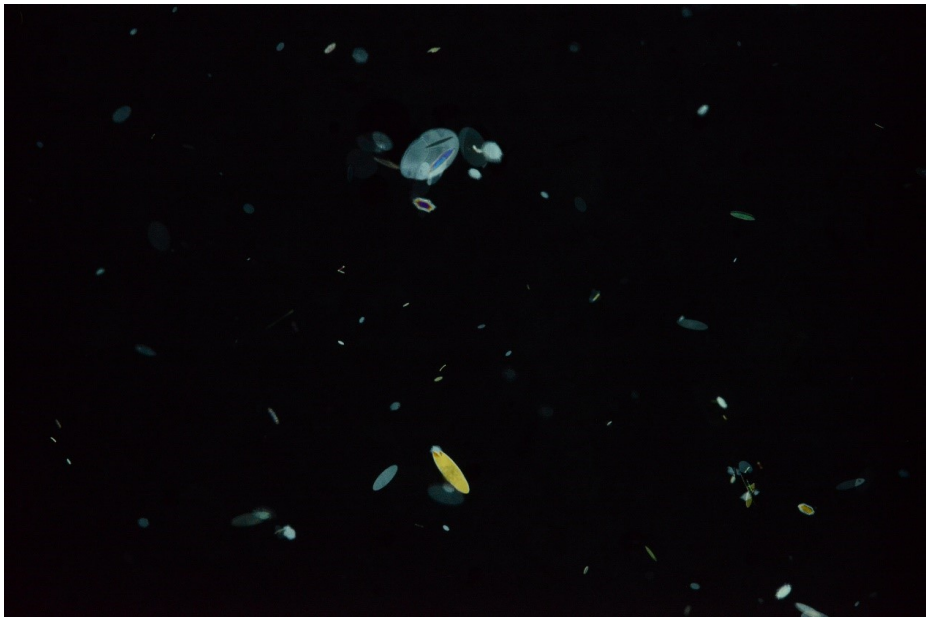

Figure 12: Raw digital images shortly after the minimum temperature was reached a) 35 ‰ b) freshwater. Image dimensions are 3.07 cm by 4.61 cm.

(a)

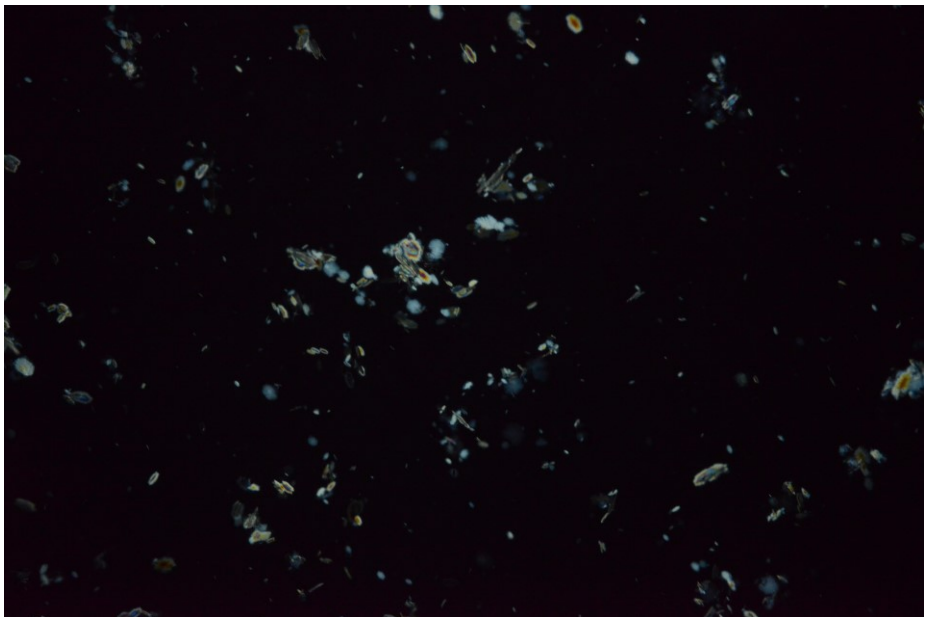

(b)

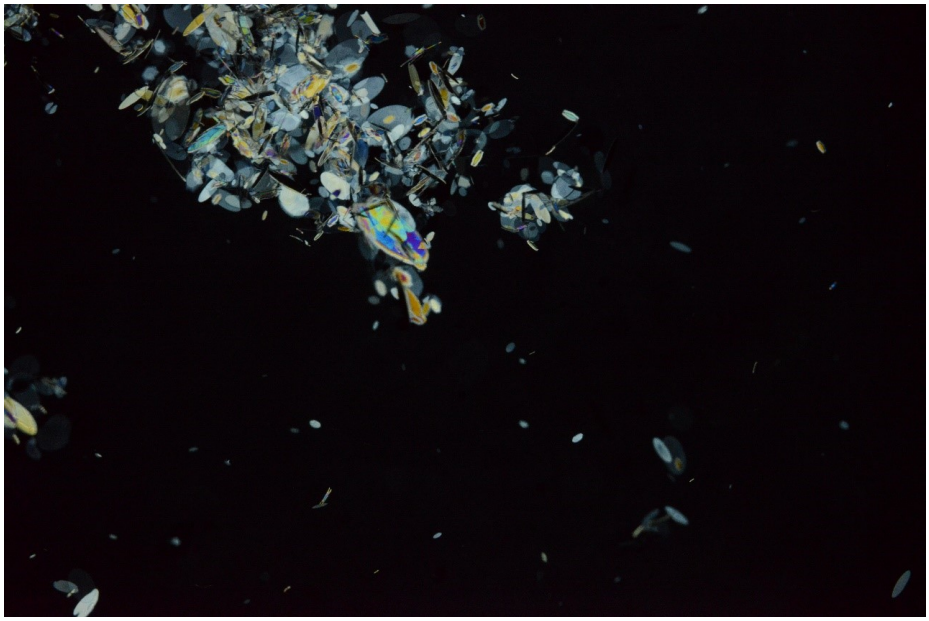

Figure 13: Raw digital images during flocculation and when temperature is rising a) 35 ‰ b) freshwater. Image dimensions are 3.07 cm by 4.61 cm.

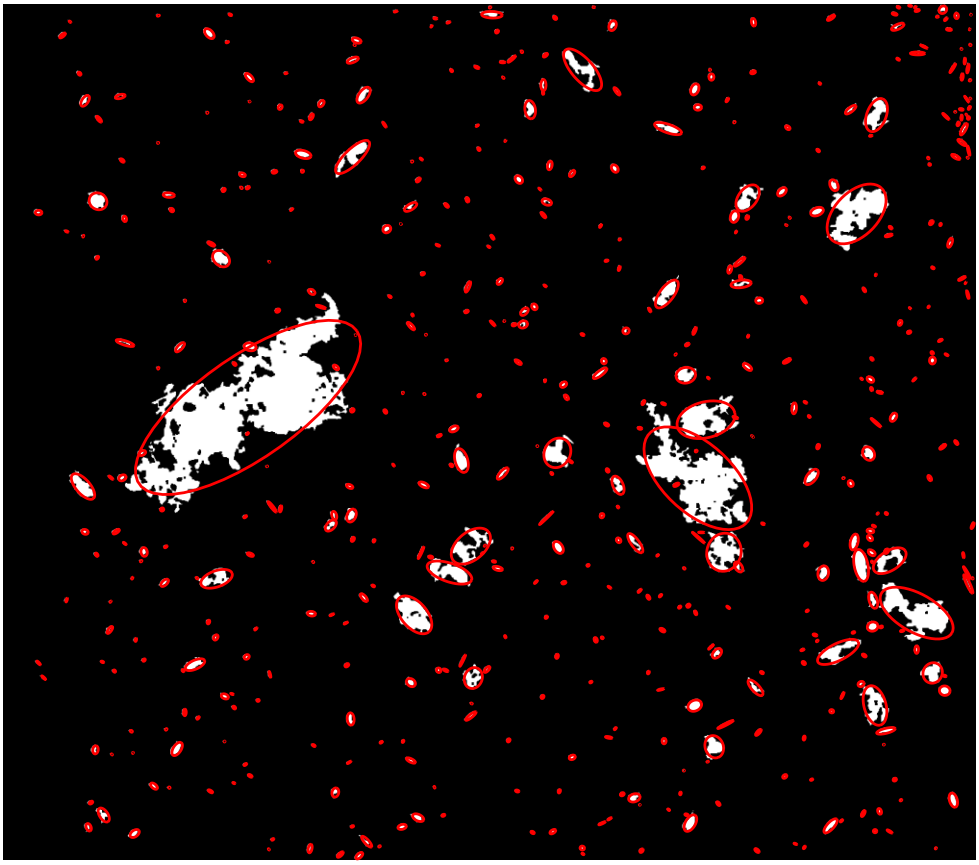

Figure 14: Binary image with superimposed fitted ellipses plotted over each detected floc.

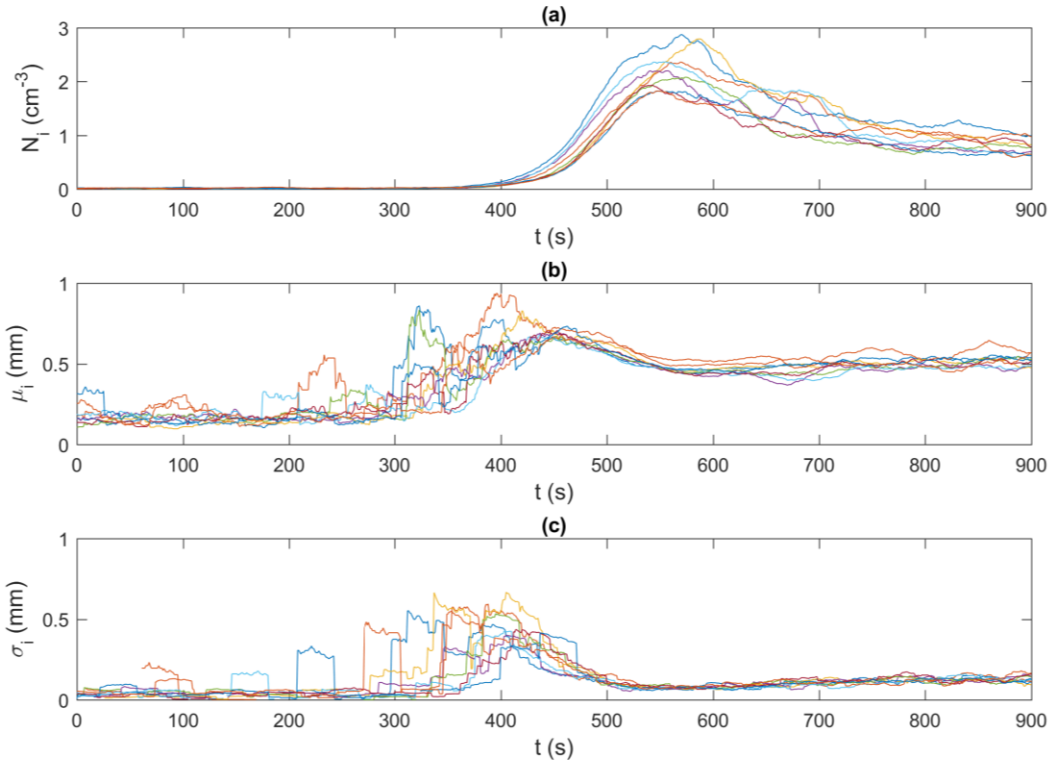

Figure 15: Time series of the 35 s moving average frazil ice particle properties for all freshwater experiments. a) N_i, the average frazil ice particle concentration, b) μ_i, the mean size of frazil ice particles, and c) σ_i, the standard deviation of the size of frazil ice particles.

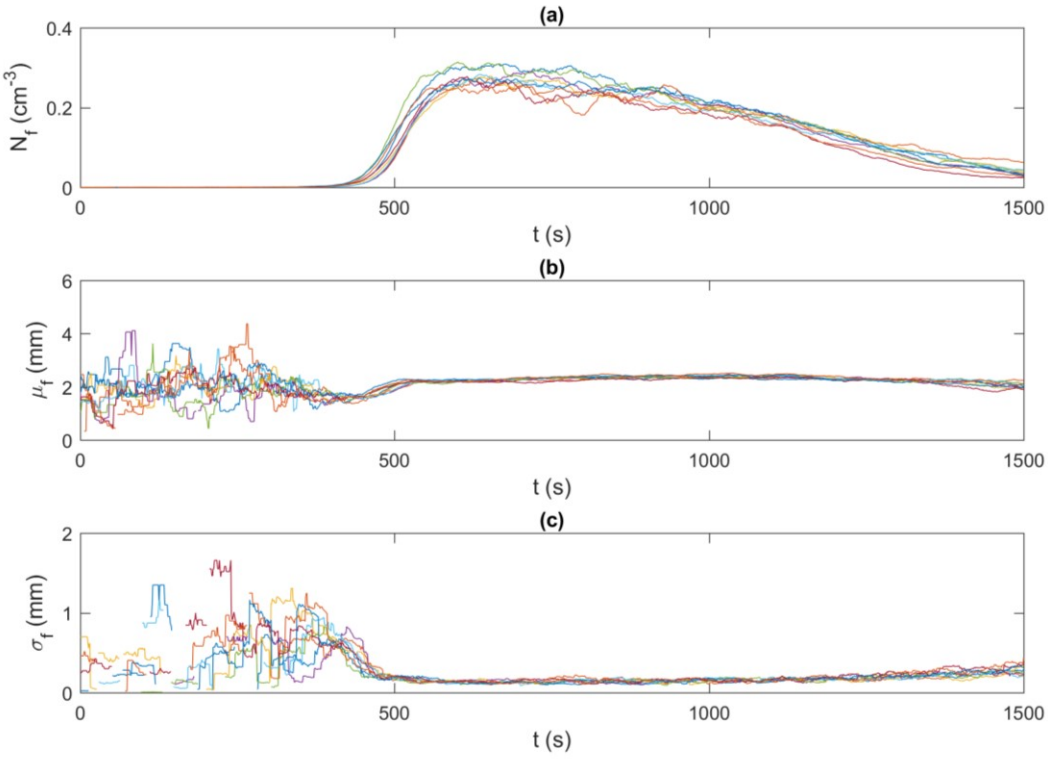

Figure 16: Time series of the 35 s moving average frazil ice floc properties for all freshwater experiments. a) N_f, the frazil ice floc concentration, b) μ_f, the mean size of frazil ice flocs, and c) σ_f, the standard deviation of the size of frazil ice flocs.

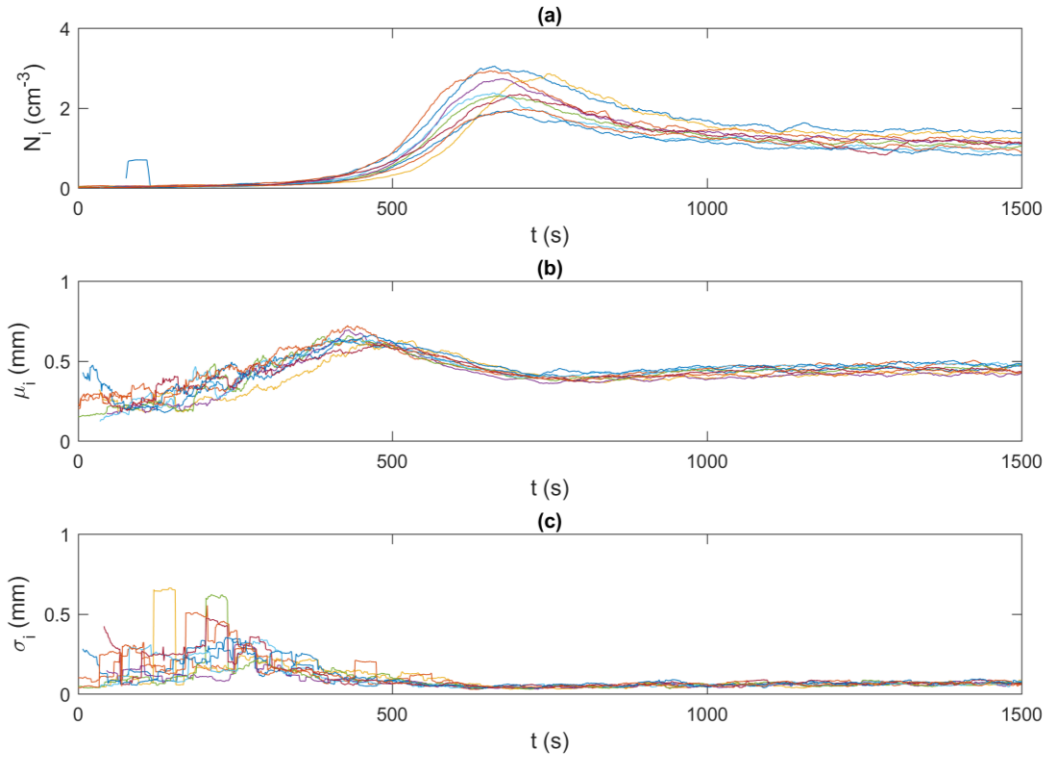

Figure 17: Time series of the 35 s moving average frazil ice particle properties for all 15 ‰ experiments. a) N_i, the frazil ice particle concentration, b) μ_i, the mean size of frazil ice particles, and c) σ_i, the standard deviation of the size of frazil ice particles.

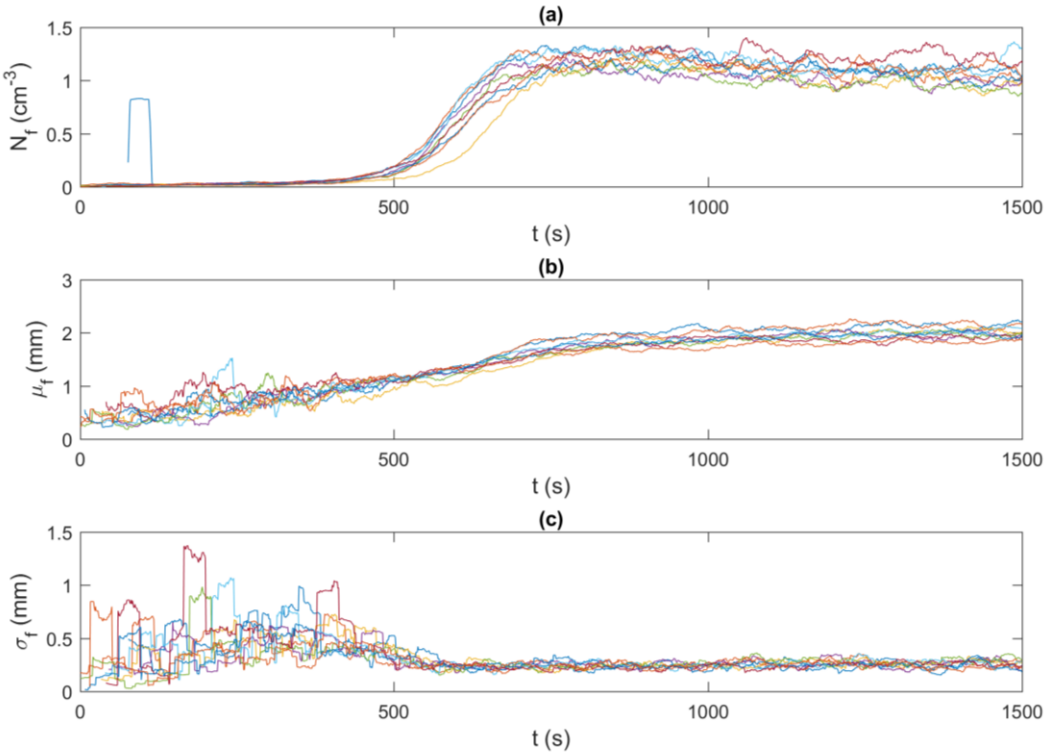

Figure 18: Time series of the 35 s moving average frazil ice floc properties for all 15 ‰ experiments. a) N_f, the frazil ice floc concentration, b) μ_f, the mean size of frazil ice flocs, and c) σ_f, the standard deviation of the size of frazil ice flocs.

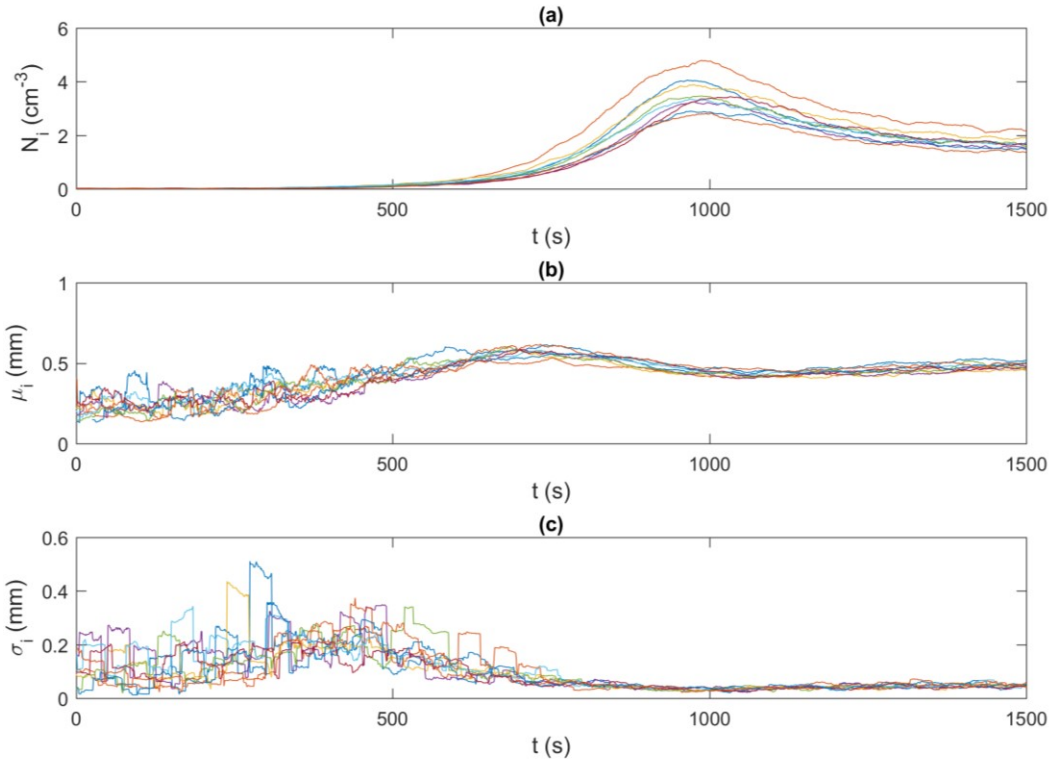

Figure 19: Time series of the 35 s moving average frazil ice particle properties for all 25 ‰ experiments. a) N_i, the frazil ice particle concentration, b) μ_i, the mean size of frazil ice particles, and c) σ_i, the standard deviation of the size of frazil ice particles.

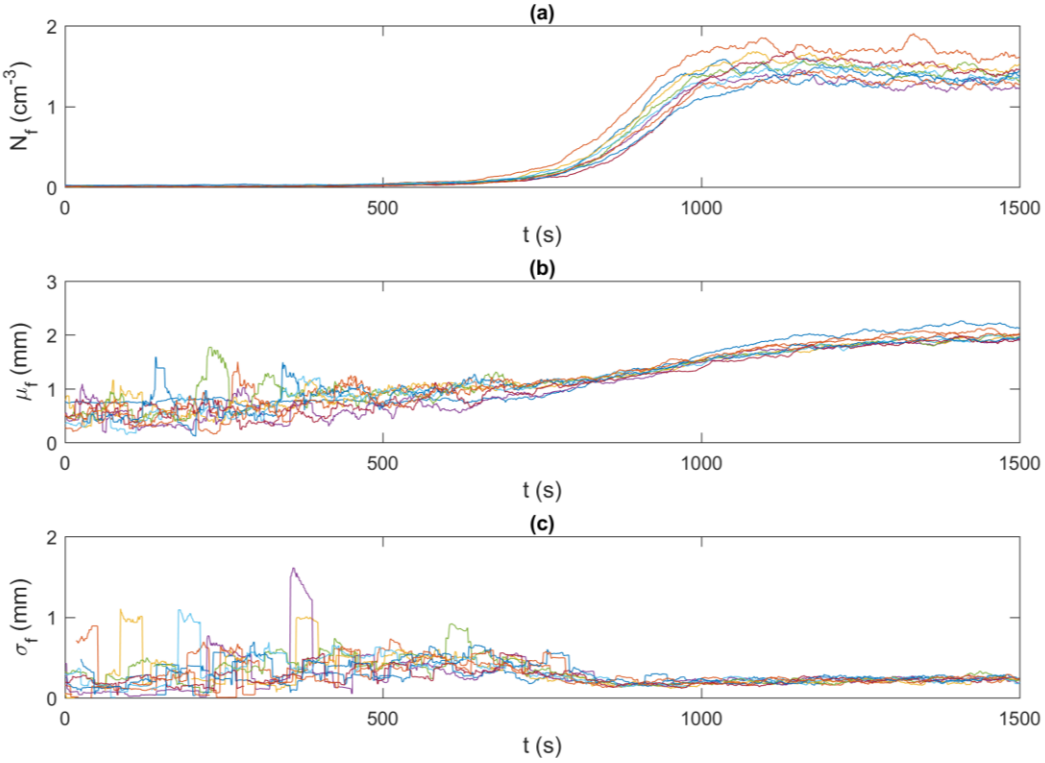

Figure 20: Time series of the 35 s moving average frazil ice floc properties for all 25 ‰ experiments. a) N_f, the frazil ice floc concentration, b) μ_f, the mean size of frazil ice flocs, and c) σ_f, the standard deviation of the size of frazil ice flocs.

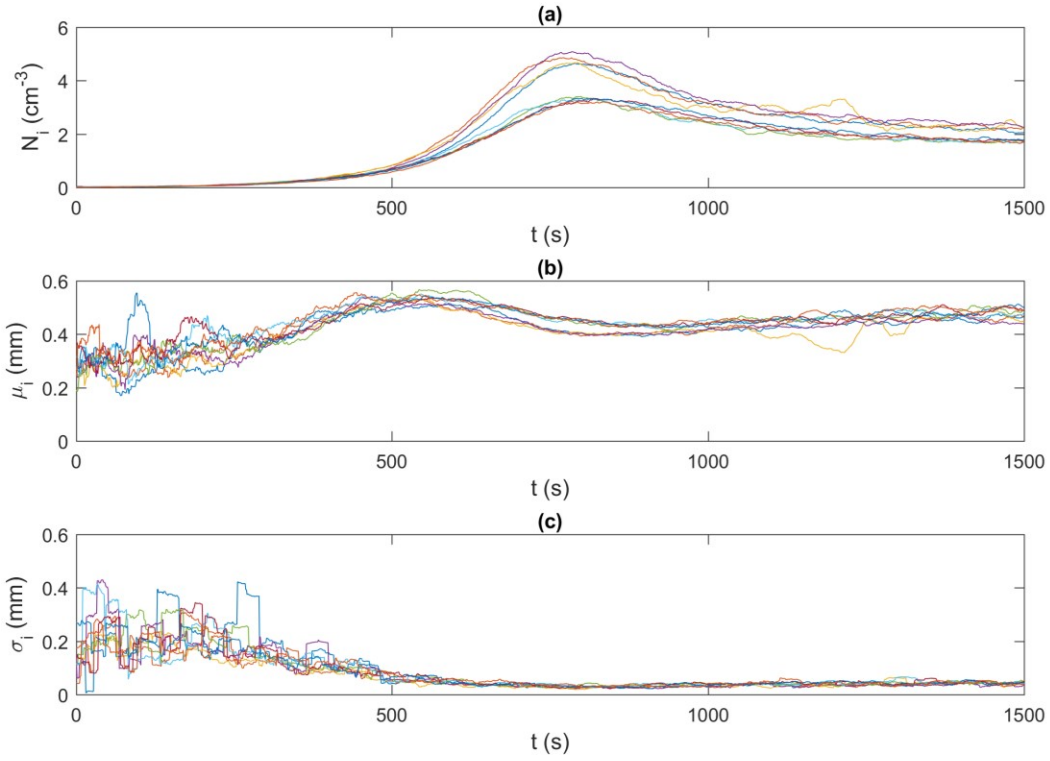

Figure 21: Time series of the 35 s moving average frazil ice particle properties for all 35 ‰ experiments. a) N_i, the frazil ice particle concentration, b) μ_i, the mean size of frazil ice particles, and c) σ_i, the standard deviation of the size of frazil ice particles.

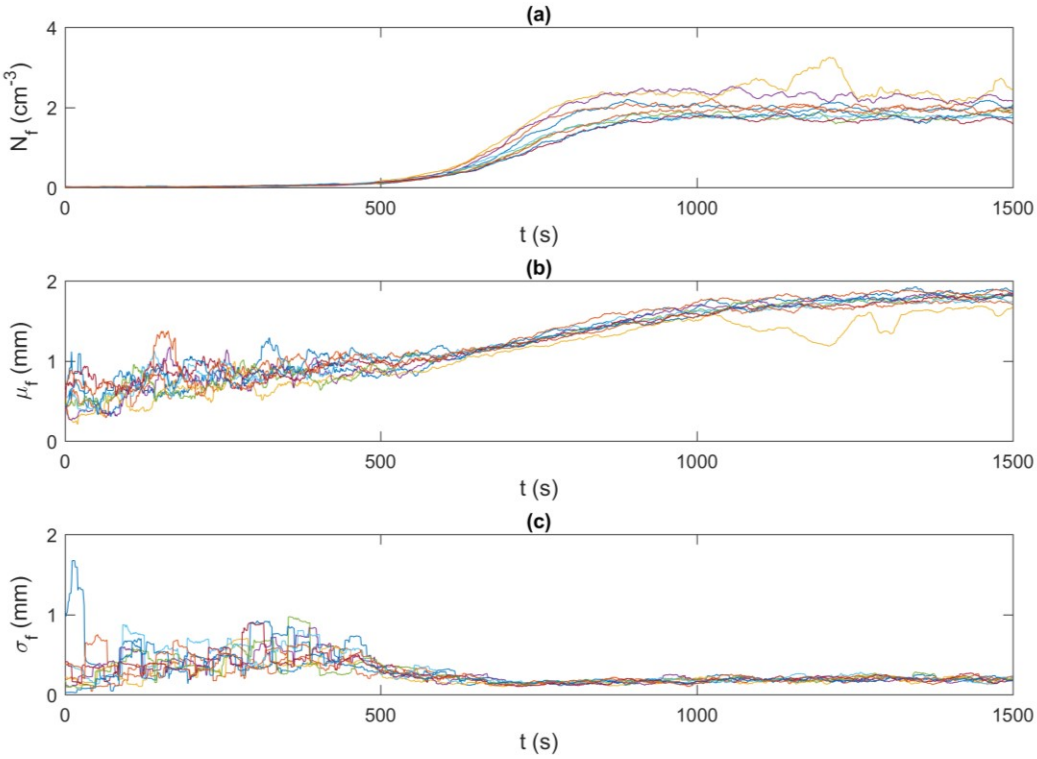

Figure 22: Time series of the 35 s moving average frazil ice floc properties for all 35 ‰ experiments. a) N_f, the frazil ice floc concentration, b) μ_f, the mean size of frazil ice flocs, and c) σ_f , the standard deviation of the size of frazil ice flocs.

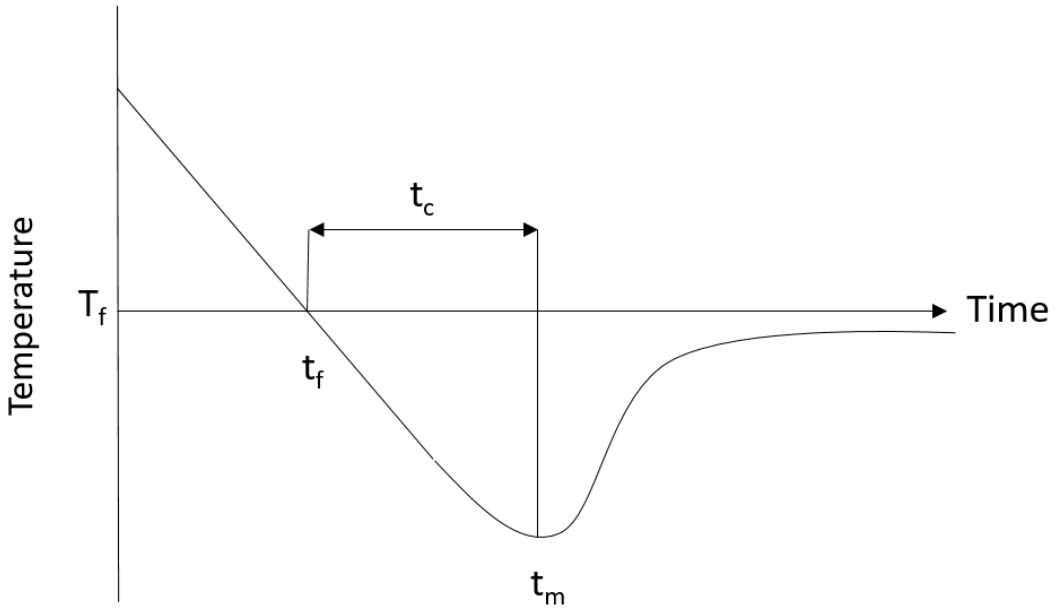

Figure 23: Typical supercooling curve with water temperature as a function of time, where t_f is the time of freezing, t_m is the time of minimum temperature, t_c is the time of cooling and T_f is the freezing temperature.

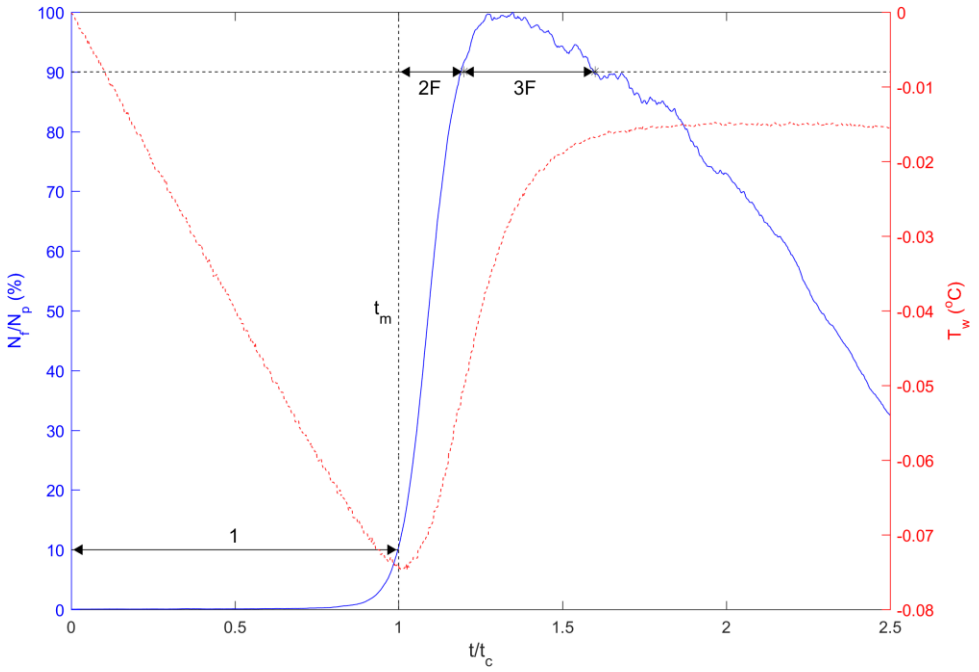

Figure 24: Dimensionless number of flocs per image as a function of dimensionless time with superimposed supercooling curve for freshwater experiments illustrating the time intervals of the different phases. N_f is the number of flocs per image, N_p is the peak number of flocs per image, T_w is the water temperature, t is the time, t_c is the time of cooling, t_f is the time of freezing, and t_m is the time of minimum temperature.

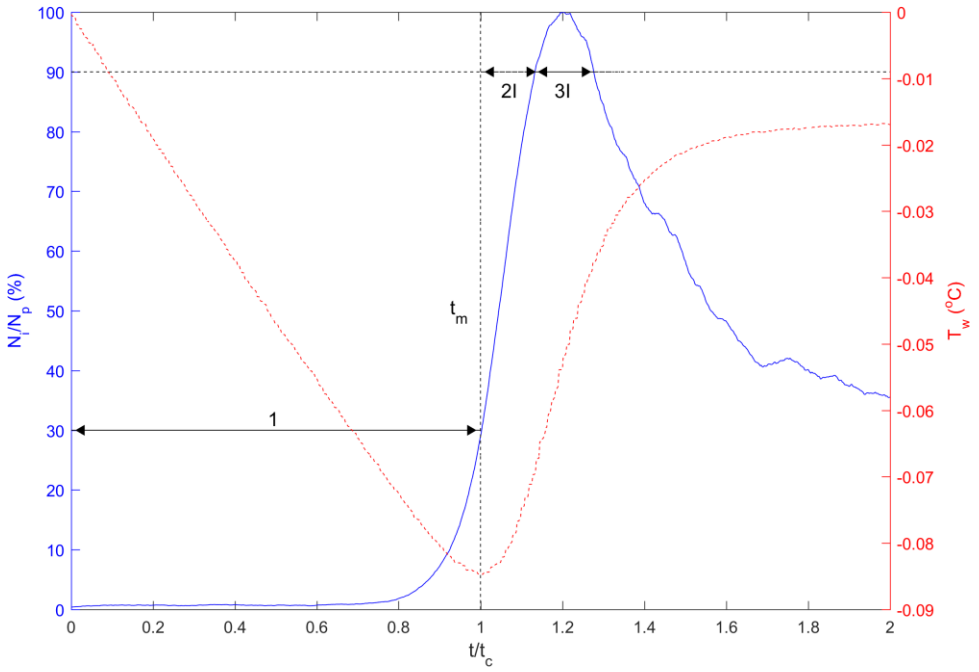

Figure 25: Dimensionless number of particles per image as a function of dimensionless time with superimposed supercooling curve for freshwater experiments illustrating the time intervals of the different phases. N_i is the number of particles per image, N_p is the peak number of particles per image, T_w is the water temperature, t is the time, t_c is the time of cooling, t_f is the time of freezing, and t_m is the time of minimum temperature.

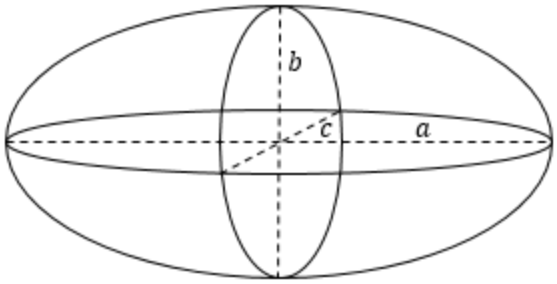

Figure 26: Sketch of an ellipsoid, where *a* is the semi-major axis length of an ellipse in 2-D, *b* is the semi-minor axis length of an ellipse in 2-D and *c* is the third semi-axis length.

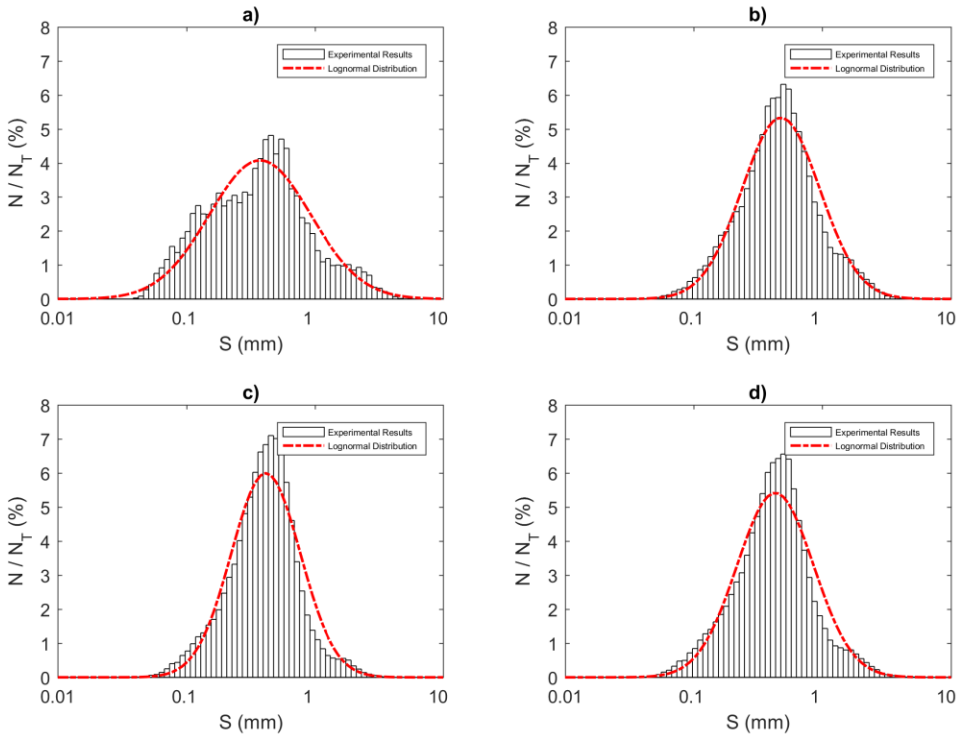

Figure 27: Frazil ice particle size distributions for freshwater for a) Phase 1, b) Phase 2I, c) Phase 3I, and d) the entire time interval (i.e. all three phases). N is the number of particles in each bin, N_T is the total number of particles, and S is the particle size.

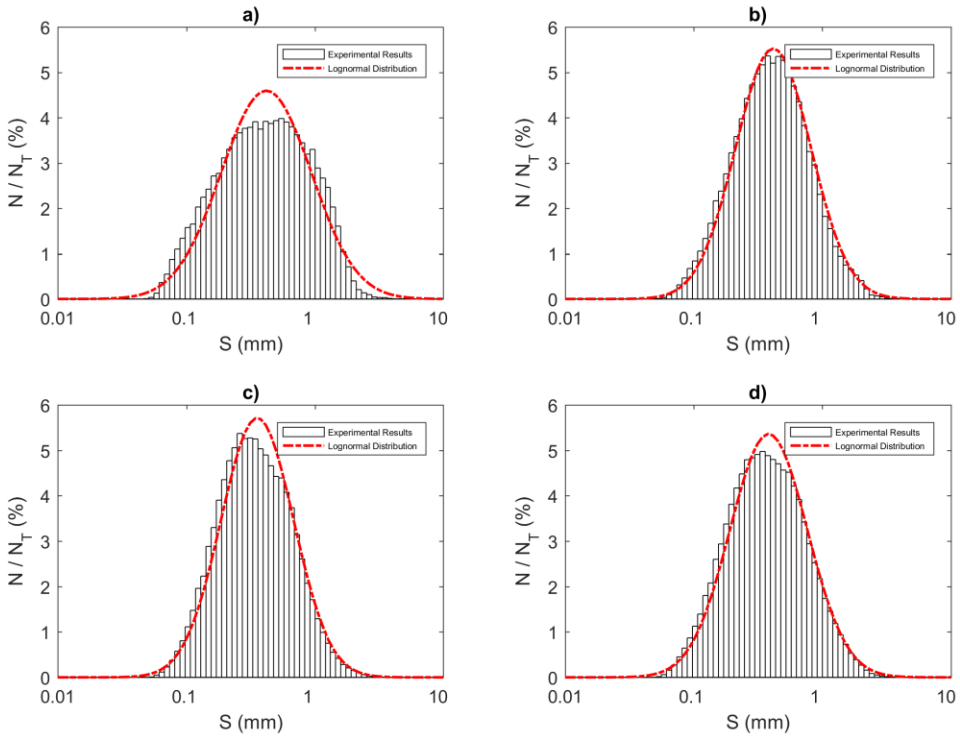

Figure 28: Frazil ice particle size distributions for 15 ‰ for a) Phase 1, b) Phase 2I, c) Phase 3I, and d) the entire time interval (i.e. all three phases). N is the number of particles in each bin, N_T is the total number of particles, and S is the particle size.

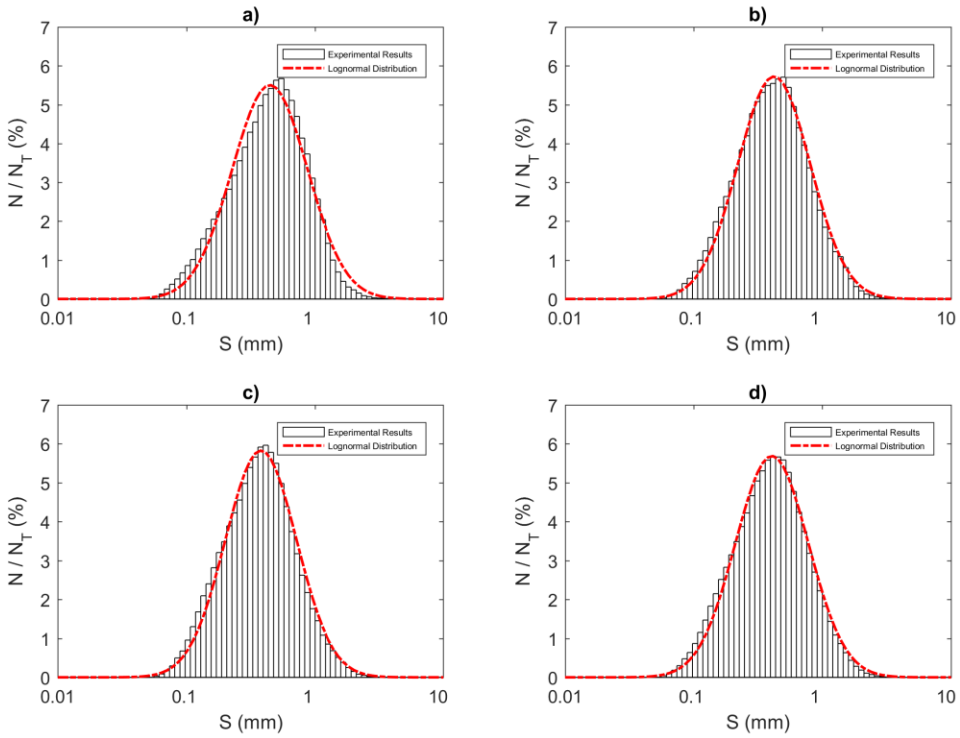

Figure 29: Frazil ice particle size distributions for 25 ‰ for a) Phase 1, b) Phase 2I, c) Phase 3I, and d) the entire time interval (i.e. all three phases). N is the number of particles in each bin, N_T is the total number of particles, and S is the particle size.

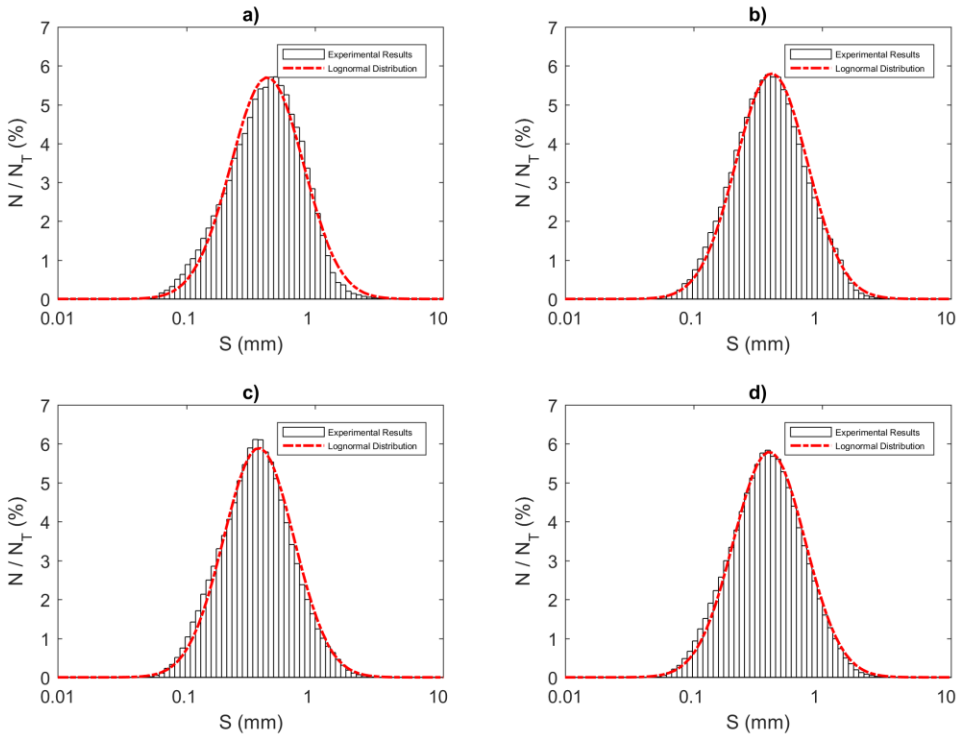

Figure 30: Frazil ice particle size distributions for 35 ‰ for a) Phase 1, b) Phase 2I, c) Phase 3I, and d) the entire time interval (i.e. all three phases). N is the number of particles in each bin, N_T is the total number of particles, and S is the particle size.

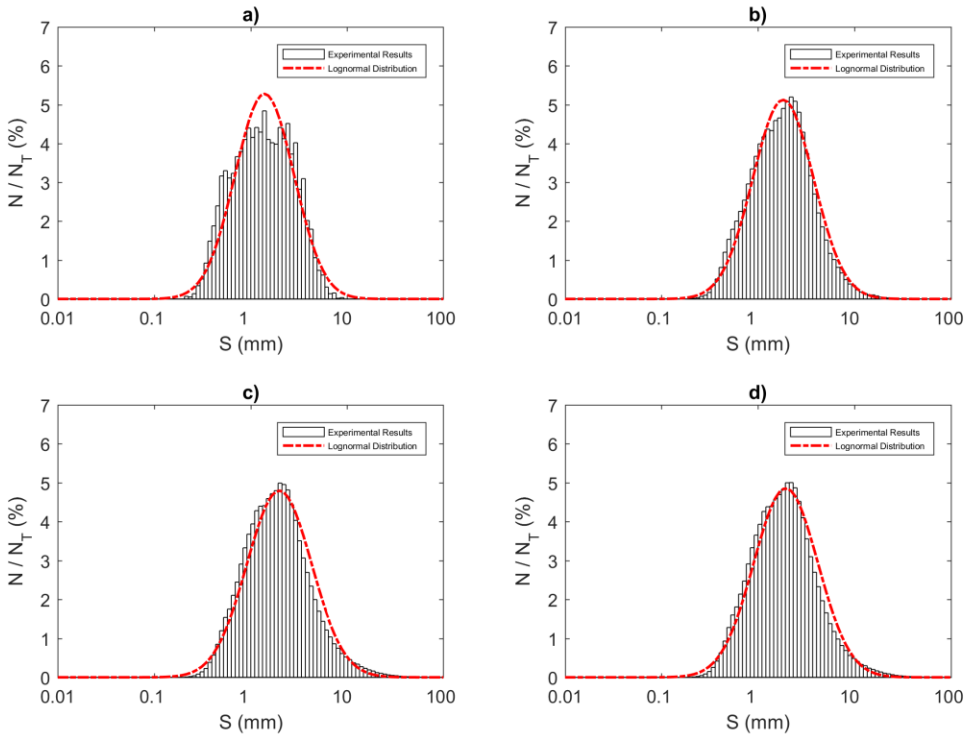

Figure 31: Frazil ice floc size distributions for freshwater for a) Phase 1, b) Phase 2F, c) Phase 3F, and d) the entire time interval (i.e. all three phases). N is the number of flocs in each bin, N_T is the total number of flocs, and S is the floc size.

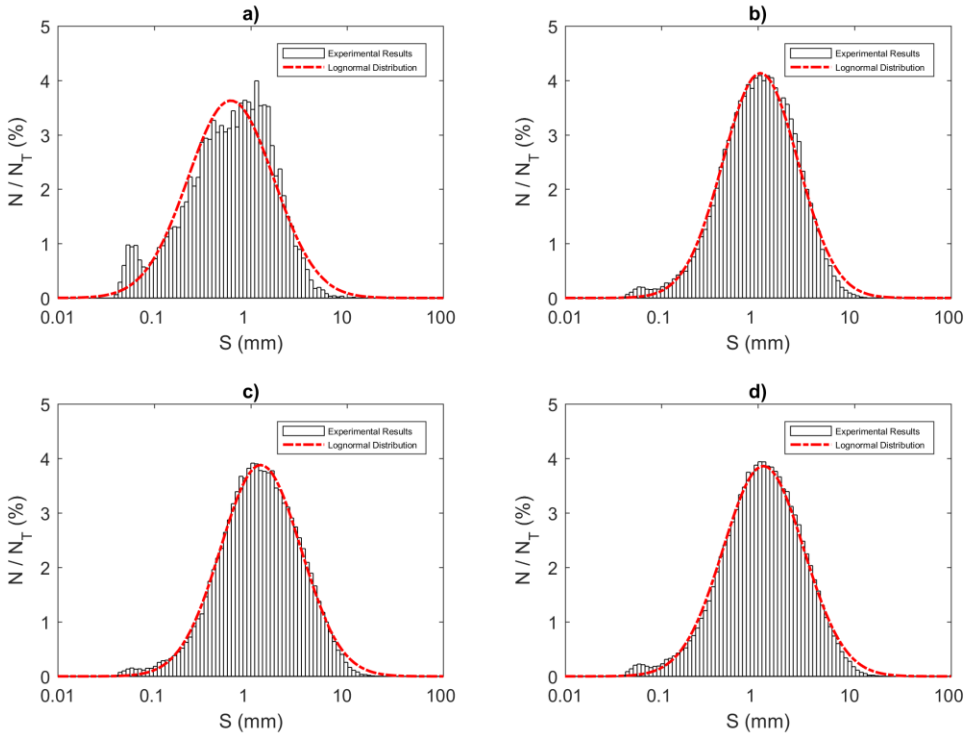

Figure 32: Frazil ice floc size distributions for 15 ‰ for a) Phase 1, b) Phase 2F, c) Phase 3F, and d) the entire time interval (i.e. all three phases). N is the number of flocs in each bin, N_T is the total number of flocs, and S is the floc size.

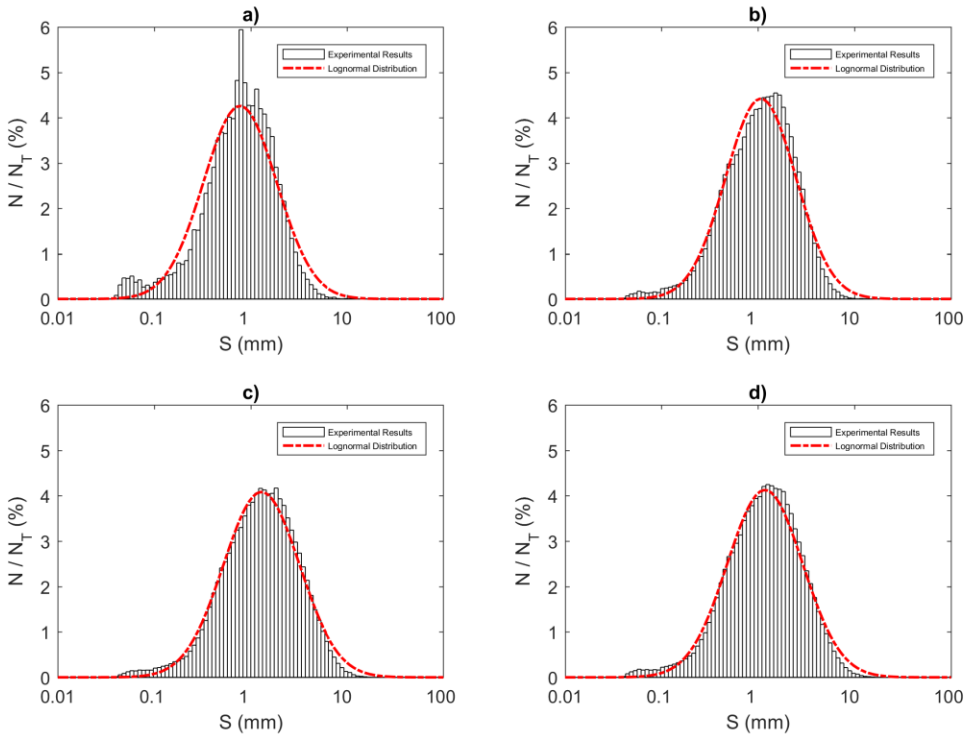

Figure 33: Frazil ice floc size distributions for 25 ‰ for a) Phase 1, b) Phase 2F, c) Phase 3F, and d) the entire time interval (i.e. all three phases). N is the number of flocs in each bin, N_T is the total number of flocs, and S is the floc size.

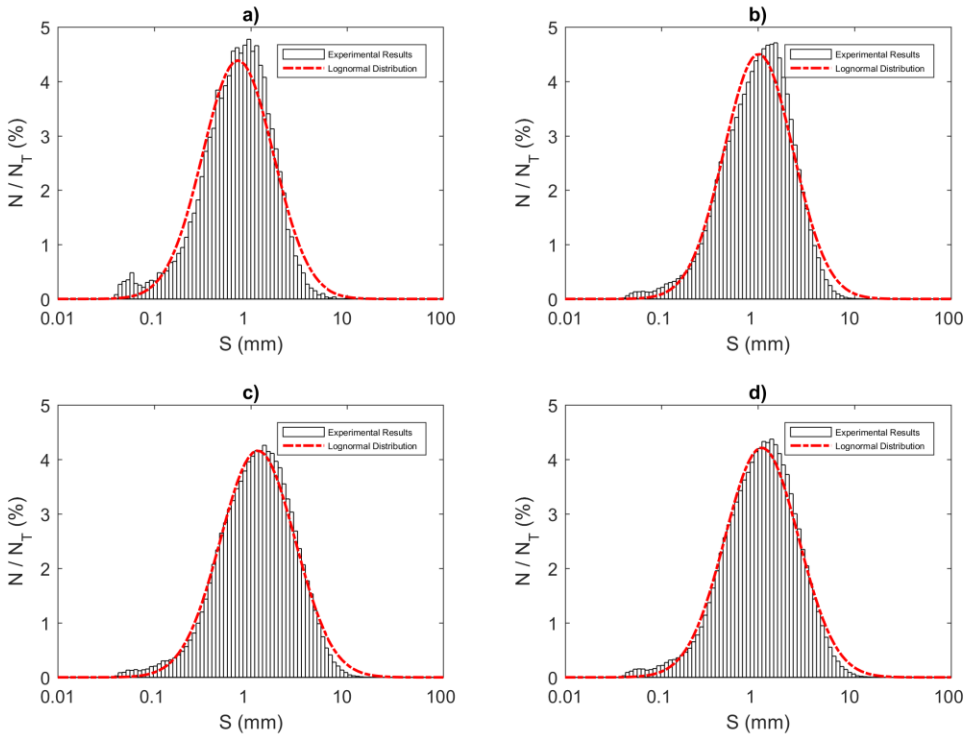

Figure 34: Frazil ice floc size distributions for 35 ‰ for a) Phase 1, b) Phase 2F, c) Phase 3F, and d) the entire time interval (i.e. all three phases). N is the number of flocs in each bin, N_T is the total number of flocs, and S is the floc size.

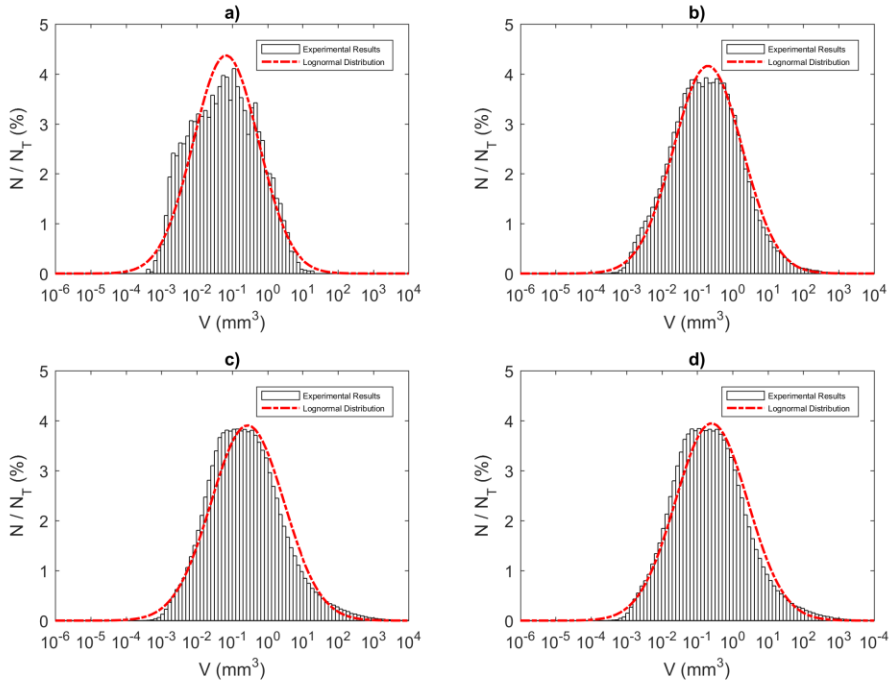

Figure 35: Frazil ice floc estimated volume distributions for freshwater for a) Phase 1, b) Phase 2F, c) Phase 3F, and d) the entire time interval (i.e. all three phases). N is the number of flocs in each bin, N_T is the total number of flocs and, V is the estimated volume of ice.

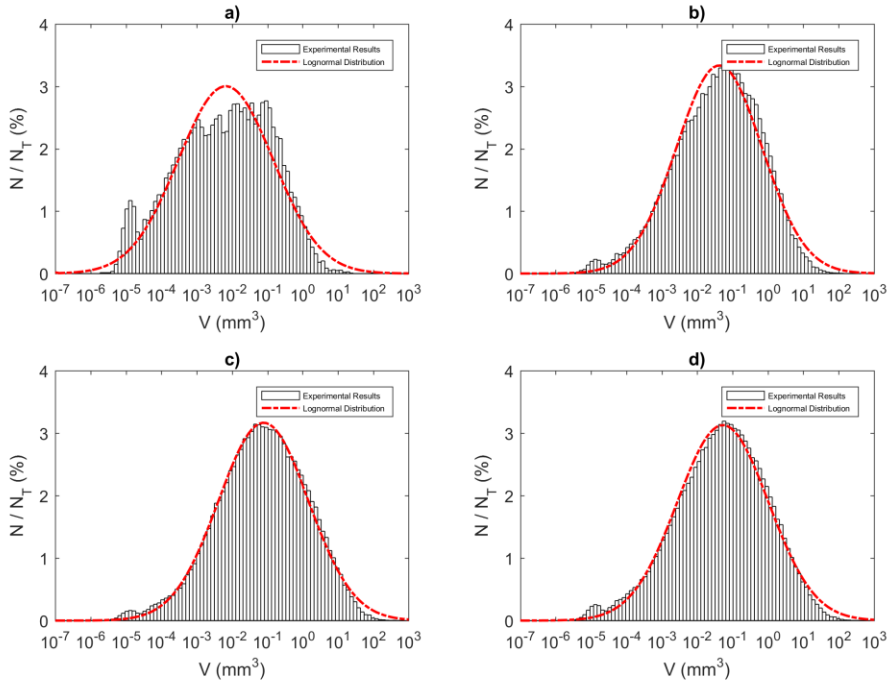

Figure 36: Frazil ice floc estimated volume distributions for 15 ‰ for a) Phase 1, b) Phase 2F, c) Phase 3F, and d) the entire time interval (i.e. all three phases). N is the number of flocs in each bin, N_T is the total number of flocs, and V is the estimated volume of ice.

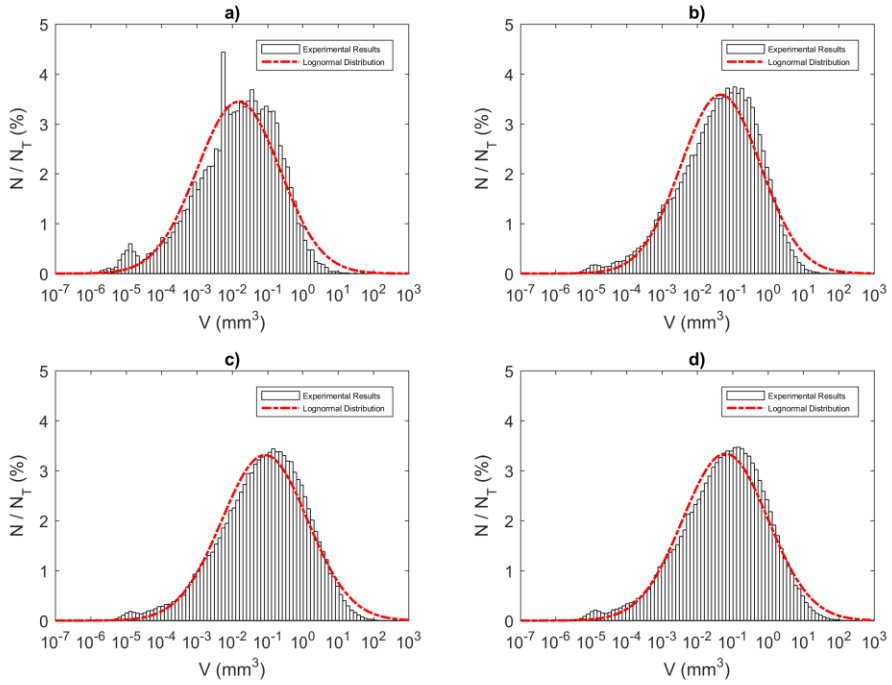

Figure 37: Frazil ice floc estimated volume distributions for 25 ‰ for a) Phase 1, b) Phase 2F, c) Phase 3F, and d) the entire time interval (i.e. all three phases). N is the number of flocs in each bin, N_T is the total number of flocs, and V is the estimated volume of ice.

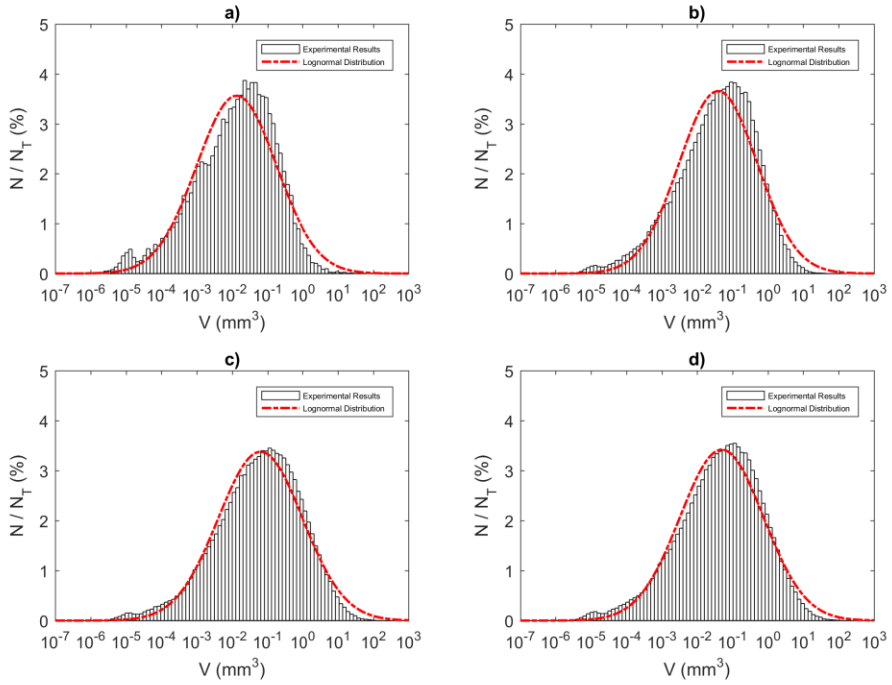

Figure 38: Frazil ice floc estimated volume distributions for 35 ‰ for a) Phase 1, b) Phase 2F, c) Phase 3F, and d) the entire time interval (i.e. all three phases). N is the number of flocs in each bin, N_T is the total number of flocs, and V is the estimated volume of ice.

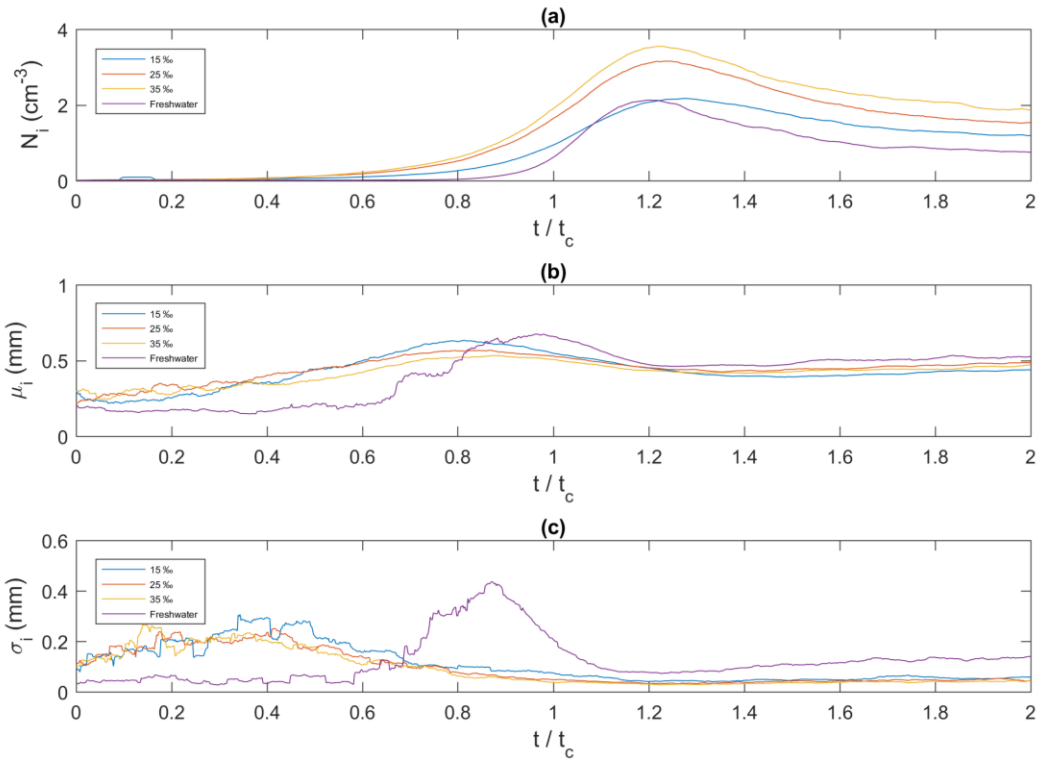

Figure 39: Non-dimensional time series of the 35 s moving average frazil ice particle properties for all four salinities. a) N_i, the average frazil ice particle concentration, b) μ_i, the mean size of frazil ice particles, and c) σ_i, the standard deviation of the size of frazil ice particles. $t/t_c = 1$ corresponds to the time of the minimum temperature on the supercooling curves.

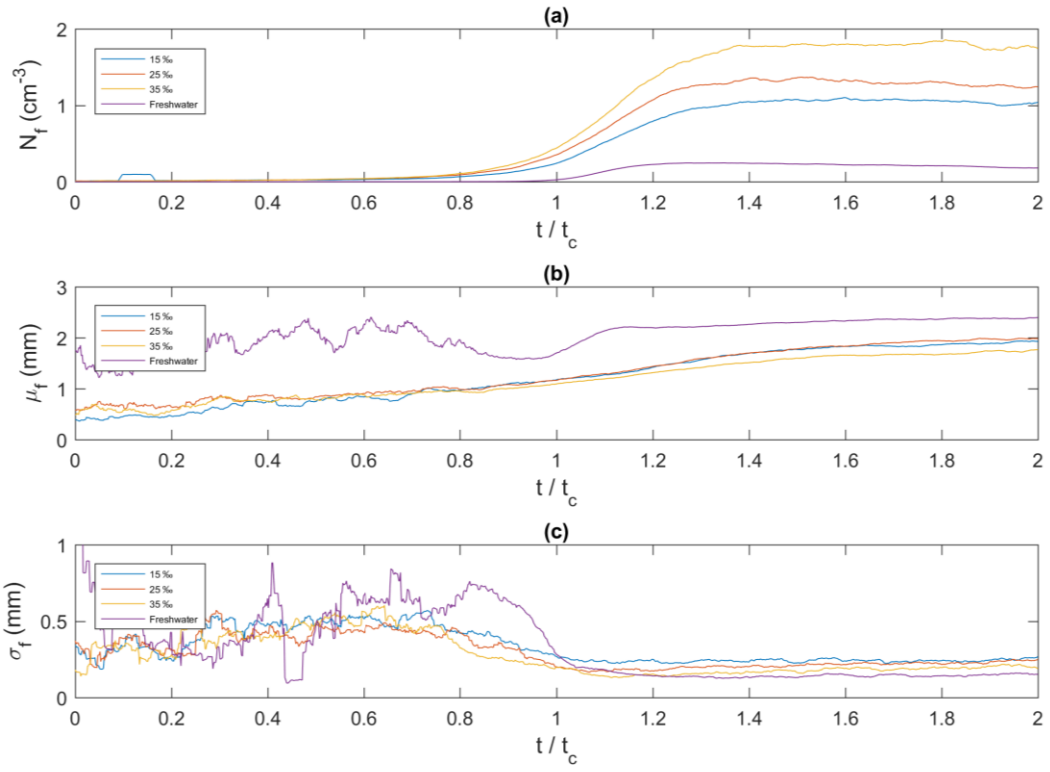

Figure 40: Non-dimensional time series of the 35 s moving average frazil ice floc properties for all four salinities. a) N_f, the average frazil ice floc concentration b) μ_f, the mean size of frazil ice flocs, and c) σ_f, the standard deviation of the size of frazil ice flocs. $t/t_c = 1$ corresponds to the time of the minimum temperature on the supercooling curves.

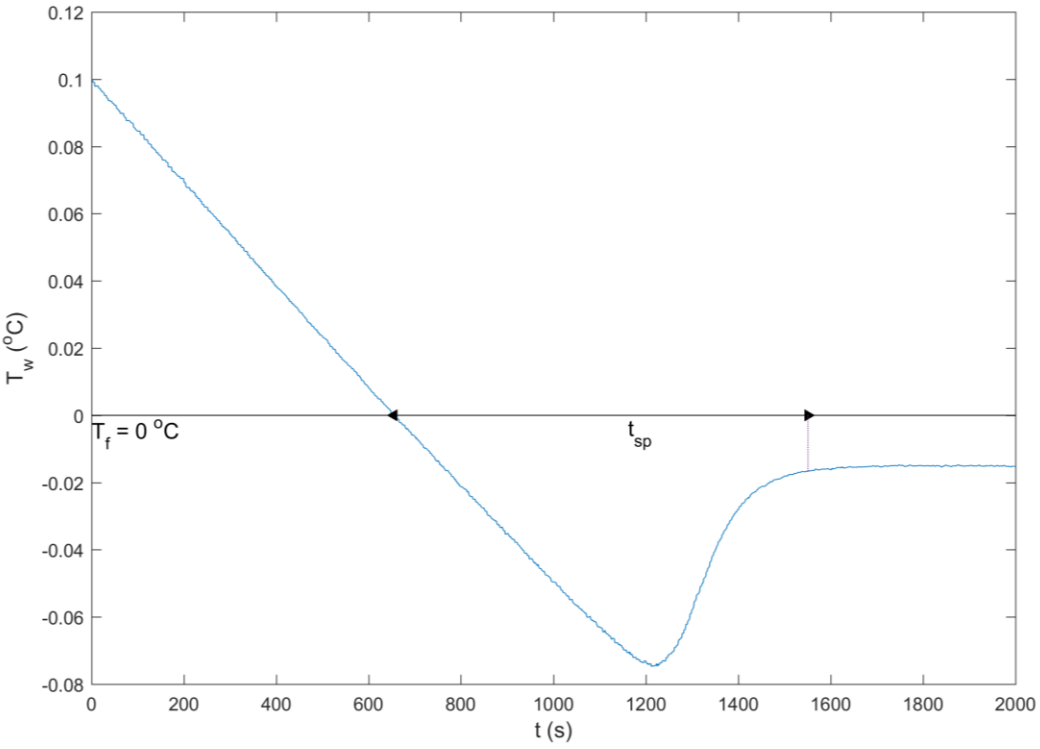

Figure 41: Average supercooling curve for freshwater experiments, where t_{sp} is the time of principal supercooling.

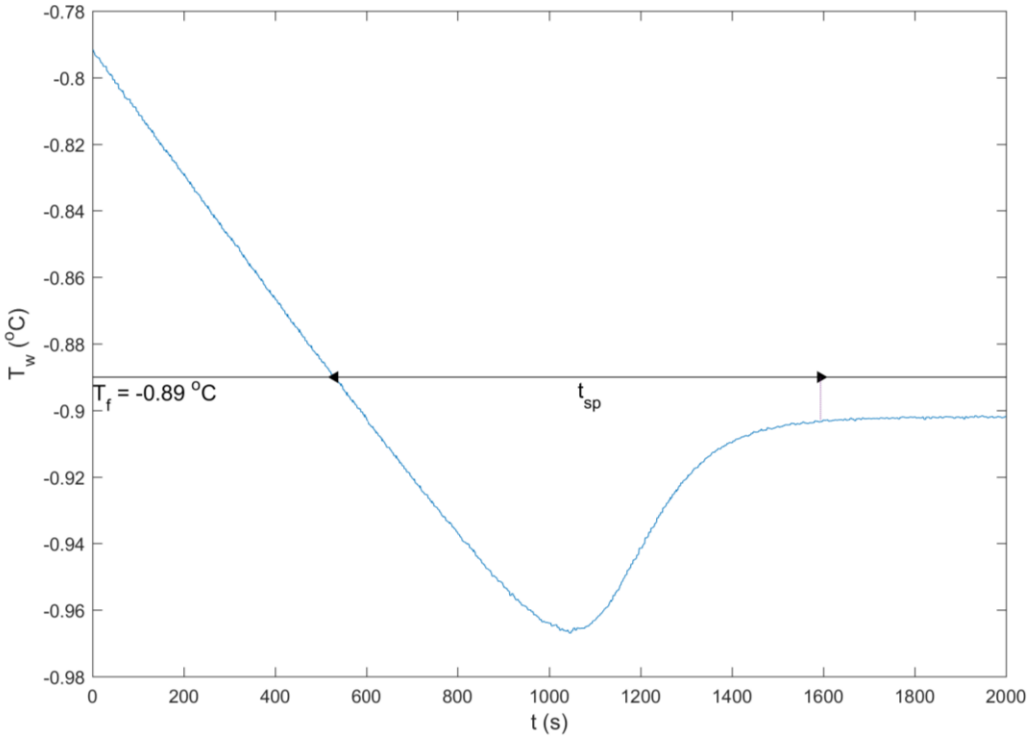

Figure 42: Average supercooling curve for 15 ‰ experiments, where t_{sp} is the time of principal supercooling.

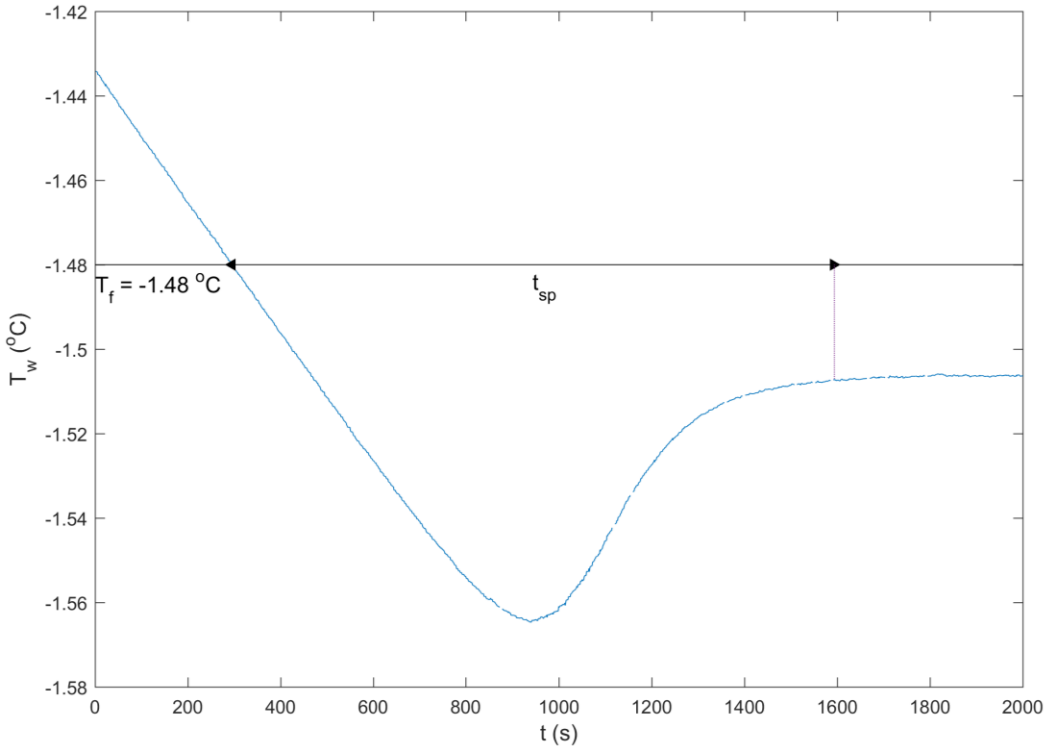

Figure 43: Average supercooling curve for 25 ‰ experiments, where t_{sp} is the time of principal supercooling.

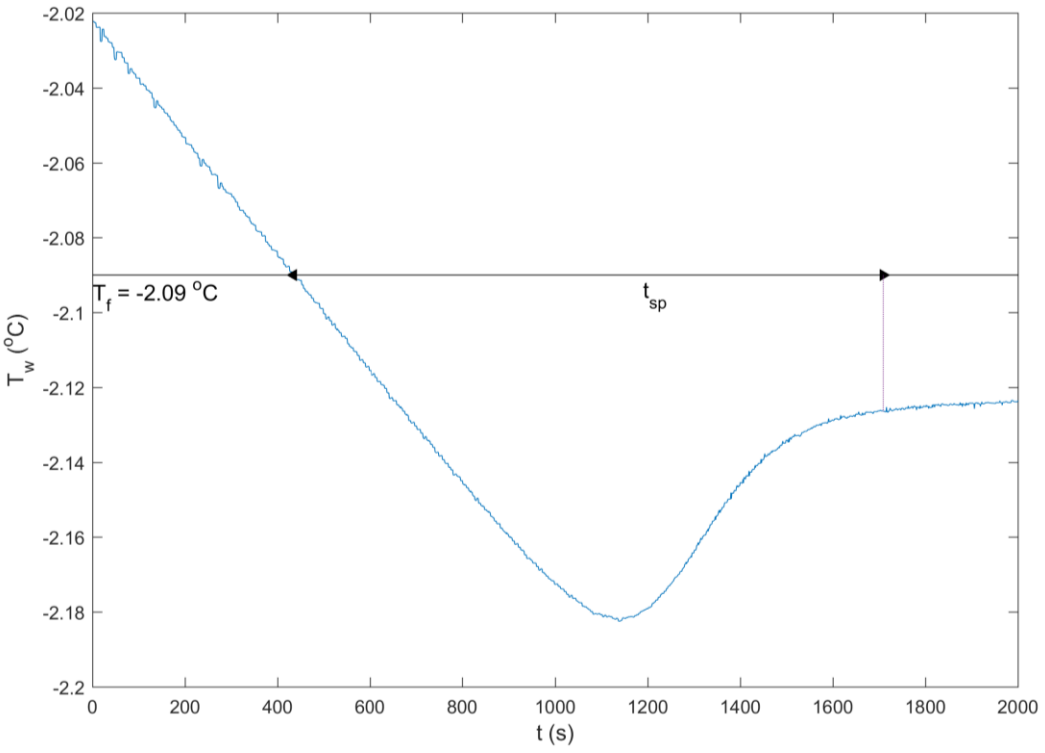

Figure 44: Average supercooling curve for 35 ‰ experiments, where t_{sp} is the time of principal supercooling.

Tables

Table 1: Summary of average difference in temperature from the RBR Solos and the Seabird

RBR ID	Average Difference in Temperature (°C)
75680	0.00067
75681	0.00289
75683	0.00076
75684	-0.00337
75686	-0.00167
75697	0.00482

Table 2: Summary of camera settings and experimental set-up for each experiment.

Setting	Set-up 1	Set-up 2	Set-up 3
Water Condition	Fresh	Saline	Fresh
Polarizers Size	Small	Small	Large
Space between Polarizers (cm)	2.2	2.2	3.5
ISO	6400	8000	6400
Shutter Speed (s)	1/2000	1/2000	1/2000
Aperture	f/25	f/29	f/25
Image Frequency	1	1	1
Camera Distance (cm)	5.7	8.7	30
Lighting System	Genaray SpectroLED Essential 360 Daylight LED Light	Genaray SpectroLED Essential 360 Daylight LED Light	Andoer FalconEyes RX-18TD 504 pcs LED Light

Table 3: Summary of experiments performed.

Experiment ID	Date	Salinity (‰)	Experimental Set-up #	Minimum Temperature (°C)	Cooling Rate (°C/min)
1-05	31-Jan-17	0	1	-0.0844	0.0118
1-06	6-Feb-17			-0.0869	0.0122
1-07	7-Feb-17			-0.0822	0.0128
1-08	8-Feb-17			-0.0875	0.0128
1-09	9-Feb-17			-0.0863	0.0122
1-10	10-Feb-17			-0.0848	0.0121
1-11	13-Feb-17			-0.0847	0.0127
1-12	14-Feb-17			-0.0870	0.0122
1-13	15-Feb-17			-0.0843	0.0121
1-14	16-Feb-17			-0.0825	0.0118
1-19	29-Mar-17	15	2	-0.9685	0.0106
1-20	30-Mar-17			-0.9679	0.0110
1-21	31-Mar-17			-0.9688	0.0112
1-22	3-Apr-17			-0.9705	0.0117
1-23	5-Apr-17			-0.9691	0.0115
1-24	6-Apr-17			-0.9701	0.0113
1-25	7-Apr-17			-0.9620	0.0109
1-26	10-Apr-17			-0.9634	0.0115
1-27	11-Apr-17			-0.9652	0.0113
1-28	19-Apr-17	35		-2.1809	0.0098
1-29	20-Apr-17			-2.1829	0.0099
1-30	21-Apr-17			-2.1846	0.0102
1-31	24-Apr-17			-2.1843	0.0097
1-33	26-Apr-17			-2.1805	0.0103
1-35	1-May-17			-2.1816	0.0090
1-36	2-May-17			-2.1790	0.0086
1-37	3-May-17			-2.1800	0.0086
1-38	4-May-17			-2.1876	0.0086
1-40	11-May-17	25		-1.5713	0.0097
1-41	12-May-17			-1.5619	0.0097
1-43	16-May-17			-1.5626	0.0093
1-44	17-May-17			-1.5686	0.0097
1-45	18-May-17			-1.5667	0.0097
1-46	19-May-17			-1.5637	0.0096
1-48	24-May-17			-1.5646	0.0088
1-49	25-May-17			-1.5601	0.0093
1-50	26-May-17			-1.5674	0.0095
1-54	19-Sep-17	0	3	-0.0775	0.0090
1-55	20-Sep-17			-0.0760	0.0090
1-56	21-Sep-17			-0.0717	0.0089
1-57	22-Sep-17			-0.0756	0.0096
1-58	25-Sep-17			-0.0811	0.0092
1-59	26-Sep-17			-0.0741	0.0090
1-60	27-Sep-17			-0.0713	0.0094

1-61	29-Sep-17			-0.0704	0.0088
1-62	2-Oct-17			-0.0789	0.0099

Table 4: Mean sizes and standard deviations of frazil ice particles during different phases and at all four salinities.

Salinity		Phase			Overall
		1	2I	3I	
Freshwater	Mean Size (mm)	0.54	0.58	0.48	0.52
	Standard Deviation (mm)	0.58	0.46	0.33	0.41
15 ‰	Mean Size (mm)	0.54	0.50	0.42	0.46
	Standard Deviation (mm)	0.43	0.36	0.30	0.35
25 ‰	Mean Size (mm)	0.53	0.49	0.44	0.48
	Standard Deviation (mm)	0.35	0.34	0.31	0.33
35 ‰	Mean Size (mm)	0.50	0.47	0.42	0.45
	Standard Deviation (mm)	0.32	0.32	0.29	0.31

Table 5: Mean sizes and standard deviations of frazil ice flocs during different phases and at all four salinities.

Salinity		Phase			Overall
		1	2F	3F	
Freshwater	Mean Size (mm)	1.68	2.28	2.65	2.57
	Standard Deviation (mm)	1.19	2.06	3.09	2.88
15 ‰	Mean Size (mm)	0.93	1.45	1.83	1.64
	Standard Deviation (mm)	0.96	1.30	1.81	1.63
25 ‰	Mean Size (mm)	1.02	1.39	1.77	1.61
	Standard Deviation (mm)	0.81	1.09	1.57	1.43
35 ‰	Mean Size (mm)	0.96	1.30	1.60	1.47
	Standard Deviation (mm)	0.82	1.01	1.40	1.28

Table 6: Sizes of the largest frazil ice flocs at all four salinities.

Salinity	95th Percentile (mm)	Maximum Floc Size (mm)	Mean Size of Flocs Larger than 95^{th} Percentile (mm)
Freshwater	6.91	95.10	11.89
15 ‰	4.82	36.22	6.77
25 ‰	4.38	23.18	5.98
35 ‰	3.96	25.19	5.38

Table 7: Estimated volumes of frazil ice flocs during different phases and at all four salinities.

Salinity		Phase			Overall
		1	2F	3F	
Freshwater	Mean Volume (mm^3)	0.40	3.01	10.67	8.79
	Standard Deviation (mm^3)	1.07	37.68	141.45	117.98
15 ‰	Mean Volume (mm^3)	0.21	0.60	1.54	1.14
	Standard Deviation (mm^3)	4.70	4.36	7.78	6.68
25 ‰	Mean Volume (mm^3)	0.15	0.39	1.08	0.82
	Standard Deviation (mm^3)	0.71	1.49	4.55	3.78
35 ‰	Mean Volume (mm^3)	0.16	0.31	0.78	0.60
	Standard Deviation (mm^3)	2.62	1.05	3.22	2.72

References

Beltaos, S. 2013. River Ice Formation. *In* 1st edition. *Edited by*S. Beltaos. Committee on River Ice Processes and the Environment, Edmonton, AB.

Cavalieri, D.J., and Martin, S. 1994. The contribution of Alaskan, Siberian, and Canadian coastal polynyas to the cold halocline layer of the Arctic Ocean. Journal of Geophysical Research, **99**(C9): 18,343-18,362.

Clark, S., and Doering, J. 2006. Laboratory Experiments on Frazil-Size Characteristics in a Counterrotating Flume. Journal of Hydraulic Engineering, **132**(1): 94–101. doi:10.1061/(ASCE)0733-9429(2006)132:1(94).

Clark, S.P., and Doering, J.C. 2009. Cold Regions Science and Technology Frazil fl occulation and secondary nucleation in a counter-rotating fl ume. Cold Regions Science and Technology, **55**(2): 221–229. Elsevier B.V. doi:10.1016/j.coldregions.2008.04.002.

Daly, S.F., and Colbeck, S.C. 1986. Frazil ice measurements in CRREL's flume facility. Available from http://login.ezproxy.library.ualberta.ca/login?url=http://search.ebscohost.com/login.aspx?direct=true&db=fih&AN=fih-EDDF7A14-8CCCE71C&site=eds-live&scope=site.

Dubé, M., Turcotte, B., and Morse, B. 2014. Cold Regions Science and Technology Inner structure of anchor ice and ice dams in steep channels. Cold Regions Science and Technology, **106**–**107**: 194–206. Elsevier B.V. doi:10.1016/j.coldregions.2014.06.013.

Galton-Fenzi, B.K., Hunter, J.R., Coleman, R., Marsland, S.J., and Warner, R.C. 2012. Modeling the basal melting and marine ice accretion of the Amery Ice Shelf. Journal of Geophysical Research, **117**(May): 1–19. doi:10.1029/2012JC008214.

Ghobrial, T.R., Loewen, M.R., and Hicks, F. 2012. Laboratory calibration of

upward looking sonars for measuring suspended frazil ice concentration. Cold Regions Science and Technology, **70**: 19–31. Elsevier B.V. doi:10.1016/j.coldregions.2011.08.010.

Ghobrial, T.R., Loewen, M.R., and Hicks, F.E. 2013. Cold Regions Science and Technology Characterizing suspended frazil ice in rivers using upward looking sonars. Cold Regions Science and Technology, **86**: 113–126. Elsevier B.V. doi:10.1016/j.coldregions.2012.10.002.

Gill, A.E. 1982. Atmosphere-Ocean Dynamics. Academic Press, Inc., San Diego, California.

Gosink, J.P., and Osterkamp, T.E. 1983. Measurements and analysis of velocity profiles and frazil ice-crystal rise veloccities. Annals of Glaciology, **4**: 79–84.

Hanley, T.O.D., and Tsang, G. 1984. Formation and properties of frazil in saline water. Cold Regions Science and Technology, **8**(3): 209–221. doi:10.1016/0165-232X(84)90052-1.

Hobbs, P.V. 1970. Ice Physics. Oxford University PRess, New York City.

Holland, P.R., and Feltham, D.L. 2005. Frazil dynamics and precipitation in a water column with depth-dependent supercooling. Journal of Fluid Mechanics, **530**: 101–124. doi:10.1017/S002211200400285X.

Jasek, M., and Pryse-phillips, A. 2015. Influence of the proposed Site C hydroelectric project on the ice regime of the Peace River 1. **655**(October 2014): 645–655.

Jenkins, A., and Bombosch, A. 1995. Modeling the effects of frazil ice crystals on the dynamics and thermodynamics of Ice Shelf Water plumes an area larger than that of the Norwegian Sea masses beneath an ice shelf were taken by MacAyeal His Oceanographic observations made near results sugg. Journal of Geophysical Research, **100**: 6967–6981.

Kalke, H., McFarlane, V., Schneck, C., and Loewen, M. 2017. Cold Regions

Science and Technology The transport of sediments by released anchor ice. Cold Regions Science and Technology, **143**(May): 70–80. Elsevier. doi:10.1016/j.coldregions.2017.09.003.

Kellerhals, R., Neill, C.R., and Bray, D.I. 1972. Hydraulic and Geomorphic Characteristics of River in Alberta. Edmonton, Alberta.

Kempema, E.W., Reimnitz, E., Clayton, J.R.J., and Payne, J.R. 1993. Interactions of frazil and anchor ice with sedimentary particles in a flume. **21**: 137–149.

Langhorne, P.J., Hughes, K.G., Gough, A.J., Smith, I.J., Williams, M.J.M., Robinson, N.J., Stevens, C.L., Rack, W., Price, D., Leonard, G.H., Mahoney, A.R., Haas, C., and Haskell, T.G. 2015. Observed platelet ice distributions in Antarctic sea ice: An index for ocean-ice shelf heat flux. Geophysical Research Letters, **42**(13): 5442–5451. doi:10.1002/2015GL064508.

Marko, J.R., Jasek, M., and Topham, D.R. 2015. Cold Regions Science and Technology Multifrequency analyses of 2011 – 2012 Peace River SWIPS frazil backscattering data. Cold Regions Science and Technology, **110**: 102–119. Elsevier B.V. doi:10.1016/j.coldregions.2014.11.006.

Martin, S. 1981. Frazil ice in rivers and oceans. Annual Review of Fluid Mechanics, **13**: 379–397. doi:10.1146/annurev.fl.13.010181.002115.

Martin, S., and Kauffman, P. 1981. A field and laboratory study of wave damping by grease ice. Journal of Glaciology, **27**(96): 283–313.

Matsumura, Y., and Ohshima, K.I. 2015. Lagrangian modelling of frazil ice in the ocean. Annals of Glaciology, **56**(69): 373–382. doi:10.3189/2015AoG69A657.

McFarlane, V., Loewen, M., and Hicks, F. 2014. Cold Regions Science and Technology Laboratory measurements of the rise velocity of frazil ice particles. Cold Regions Science and Technology, **106**–**107**: 120–130. Elsevier B.V. doi:10.1016/j.coldregions.2014.06.009.

McFarlane, V., Loewen, M., and Hicks, F. 2015. Cold Regions Science and

Technology Measurements of the evolution of frazil ice particle size distributions. Cold Regions Science and Technology, **120**: 45–55. Elsevier B.V. doi:10.1016/j.coldregions.2015.09.001.

McFarlane, V., Loewen, M., and Hicks, F. 2017. Cold Regions Science and Technology Measurements of the size distribution of frazil ice particles in three Alberta rivers. Cold Regions Science and Technology, **142**(March): 100–117. Elsevier. doi:10.1016/j.coldregions.2017.08.001.

Morse, B., and Richard, M. 2009. Cold Regions Science and Technology A fi eld study of suspended frazil ice particles. Cold Regions Science and Technology, **55**(1): 86–102. Elsevier B.V. doi:10.1016/j.coldregions.2008.03.004.

Omstedt, A. 1985. Modelling frazil ice and grease ice froamtion in the upper layers of the ocean. Cold Regions Science and Technology, **11**: 87–98.

Osterkamp, T.E. 1978. Frazil Ice Formation: A Review.

Ramanujan, S. 1914. Modular equations and approximations to pi. Quarterly Journal of Mathematics, **45**: 350–372.

Richard, M., Morse, B., and Daly, F. 2011. QUANTIFYING SUSPENDED FRAZIL ICE USING MULTI-FREQUENCY. **1117**(September 2010): 1106–1117. doi:10.1002/rra.

She, Y., Kemp, J., Richards, L., and Loewen, M. 2016. Investigation into freezing point depression in stormwater ponds caused by road salt. Cold Regions Science and Technology, **131**: 53–64. Elsevier B.V. doi:10.1016/j.coldregions.2016.09.003.

Skyllingstad, E.D. 2001. Turbulence Beneath Sea Ice and Leads: A coupled Sea Ice/Large- Eddy Simulation Study. Journal of Geophysical Research, **106**(C2): 2477–2497.

Smedsrud, L.H., and Jenkins, A. 2004. Frazil ice formation in an ice shelf water plume. Journal of Geophysical Research, **109**(December 2003): 1–15.

doi:10.1029/2003JC001851.

Smedsrud Henrik, L.H. 2001. Frazil-ice entrainment of sediment: Large-tank laboratory experiments. Journal of Glaciology, **47**(158): 461–471. doi:10.3189/172756501781832142.

Ushio, S., and Wakatsuchi, M. 1993. A laboratory study on supercooling and frazil ice production processes in winter coastal polynyas. **98**(93): 321–328.

Weeks, W.F. 2010. On Sea Ice. *In* 1st edition. University of Alask Press, Fairbanks, Alaska.

Ye, S.Q., Doering, J., and Shen, H.T. 2004. A laboratory study of frazil evolution in a counter-rotating flume. Canadian Journal of Civil Engineering, **31**(6): 899–914. doi:10.1139/l04-056.

Appendix A: List of Matlab Functions used for Image Processing

frazilsize_“date”	Uses binary images created in discextents to determine the properties of interest of the objects using built in functions. These properties are used to assess whether the object is an particle or floc.
discextents	Converts raw images to binary images using threshold, dilates and erodes the objects, removes any objects touching the border of the image.
runensembleaverage	Loads data from frazil _"date" for a set of experiments. Using functions described below. Produces summary of statistics for flocs or particles.
supercoolshift	Processes supercooling data and produces figure of supercooling curves aligned at the freezing point.
evolvedists	Processes floc sizes to produce particle size and floc size distributions for various time intervals. Returns properties of object sizes.
evolvedists_vol	Processes floc volumes to produce particle size and floc size distributions for various time intervals. Returns properties of floc volumes
evolvedists_ecc	Processes floc properties to compute eccentricity properties of the flocs.
flocscombined	Loads data from runensembleaverage to produce combined dimensionless time ensemble average figures for flocs.
individualcombined	Loads data from runensembleaverage to produce combined dimensionless time ensemble average figures for particles.
largeflocs	Processes data from runemsembleaverage to produce property statistics for large flocs.
imageicevolumes	Processes data from runesembleaverage to estimate volumes of ice contained in the images.
repeatability	Produces figures of ensemble averages of a a set of experiments.